2017

Spatial Centering of a Quadcopter in an Underground Coal Mine

Jonathan Itschner

Spatial Centering of a Quadcopter in an Underground Coal Mine

Jonathan Itschner

Thesis submitted to the
Benjamin M. Statler College of Engineering and Mineral Resources
at West Virginia University
in partial fulfillment of the requirements
for the degree of

Master of Science
in
Electrical Engineering

Roy S. Nutter, Ph.D., Chair
Powsiri Klinkhachorn, Ph.D.
Vinod K. Kulathumani, Ph.D.

Lane Department of Computer Science and Electrical Engineering

Morgantown, West Virginia
2017

Keywords: LEDDAR, drone, mine, PID, quadcopter

Abstract

Spatial Centering of a Quadcopter in an Underground Coal Mine

Jonathan Itschner

The recent proliferation of smaller and more affordable sensing and computing has contributed to an increased availability of unmanned aerial vehicles, UAV's. Specifically, quadrotor platforms have become popular due to their low cost, versatility, and relative ease of operation. There are a variety of applications for this type of aerial vehicle, ranging from hobbyist photography to search and rescue operations. This thesis documents the feasibility of using a quadrotor UAV within the confined space of an underground coal mine during an emergency. Additionally, this paper notes in the Appendix an experiment to remotely operate a quadcopter that is located underground. This work specifies the equipment used to operate down an eight inch bore hole in terms of radios, fiber optic cables, and video hardware. The operator and quadcopter were located 50 feet apart in the experiment.

One of the most significant challenges of operating a quadcopter in an underground coal mine is collision avoidance. The automation of basic spatial centering in the underground coal mine would lessen the burden on the operator and help prevent collisions. Many spatially aware quadcopter systems already exist, but widely rely on GPS signals as a way to determine position. GPS signals are very weak radio signals that cannot penetrate into the earth. The below-ground nature of an underground coal mine precludes the use of GPS for positioning the craft. Due to this limitation, it became necessary to explore unique sensing solutions that would allow for the spatial centering of the quadcopter while operating in an underground environment.

The ability for the craft to maintain a distance from its surroundings through the use of a light-based sensor was analyzed. Sensors were placed on the bottom and side of the quadcopter, and the performance of the control system was observed. Altitude was maintained with a steady state error of 4%, and the response to a step change in ground height resulted in a 10% lower overshoot than simulation. Simultaneously, distance was maintained from the side with a steady state error of 7.8%. The work presented in this document serves as validation for the basic spatial awareness and crash avoidance capability of a quadcopter operating without GPS in an underground coal mine while controlled remotely down an eight inch borehole.

Acknowledgments

I would like to thank my advisor, Dr. Nutter, for his invaluable input and guidance. Without him, I would not have been able to complete my research in a timely manner. His steadfast direction kept my efforts focused on the scope of the research and helped to convey my findings in meaningful ways.

I would also like to thank Dr. Klinkhachorn and Dr. Vinod, who indirectly contributed an incredible amount to my research. Manipulating the hardware and software of the quadcopter was possible only by calling upon the knowledge that I gained while I was their student.

I would also like to acknowledge the Lane Department for their financial support throughout my time in graduate school. Without their assistance none of this would have been possible.

In addition, I would like to acknowledge the financial assistance provided by the Arch Coal Inc. Endowment for Mine Health and Safety Research in CEMR. My research assistantship in the summer of 2016 was an invaluable experience that directly contributed to my understanding of the research presented in this thesis.

Finally, I thank my family for their continued support during my research. Their constant encouragement and support was sometimes the only thing that kept me motivated to continue. I would not be where I am today without them. Thank you.

Contents

List of Tables

List of Figures

Chapter 1

Introduction

The operation of quadcopter (UAV) within a confined space results in a set of unique challenges for safe and successful operation. In the case of an underground mine, it is important to consider the distance between the quadcopter and the surrounding ribs, roof, and floor during operation to prevent collisions. Due to the nature of the operating environment in a mine, traditional methods for altitude and position holding such as GPS and barometers are ineffective. This paper explores the performance of a relatively low cost light-based distance sensing approach to ensure the positional centering of the quadcopter during operation in a mine.

1.1 Motivational Scenario

Assessing the condition of an underground coal mine can be of critical importance after a fire or other emergency that might include a roof collapse or a rib roll. Under the worst conditions, bore holes are used to drill down from the surface into the mine, and a camera and/or sensors are used to observe the condition of the mine. One example of this type of borehole is seen in Figure 1.1, which shows a shaft drilled 240 feet down into the Quecreek mine to establish communications and provide fresh air to trapped coal miners. This type of borehole is often used during mine rescue operations. During a coal mine fire, it can be used to gain insight on the air and fire conditions inside the mine. Of great interest is the evaluation of the atmospheric conditions in the mine (e.g. carbon monoxide, oxygen, etc.),

especially since air quality is one of the most life threatening and dangerous aspects of an underground coal mine, especially during emergency conditions.

Figure 1.1: Quecreek Mine Airshaft [4]

Figure 1.2: An eight inch pipe used for borehole casing

The primary limitation of this approach is the small observable area of the mine that is limited to the exit of the borehole. Introducing a UAV into the mine via the borehole could allow for exploration and atmospheric measurements well beyond the bottom of the borehole. The UAV should be able to move away from the bottom of the borehole and provide a much broader reading of the mine environment around that location. The UAV used for mine exploration should ideally be able to carry atmospheric sensing equipment and a camera capable of both visible and infrared images. To allow for exploration beyond the bottom of the borehole and further into the mine, a radio repeater network would be necessary for communication due to the line-of-sight propagation of radio frequency signals in an underground mine. An automated battery swapping mechanism could also be used to allow for longer deployments while in the mine, and potentially enable even longer flight distances from the bottom of the borehole [4].

The UAV used for underground mine exploration will need to fit down an eight inch bore hole, send live video to the pilot, and be controlled by the pilot who would be located above-ground. Since radio frequencies used to control quadcopter do not propagate through the ground, a communication solution must be used to allow for above-ground control of the quadcopter in the mine and for video and data to be sent from underground to the surface.

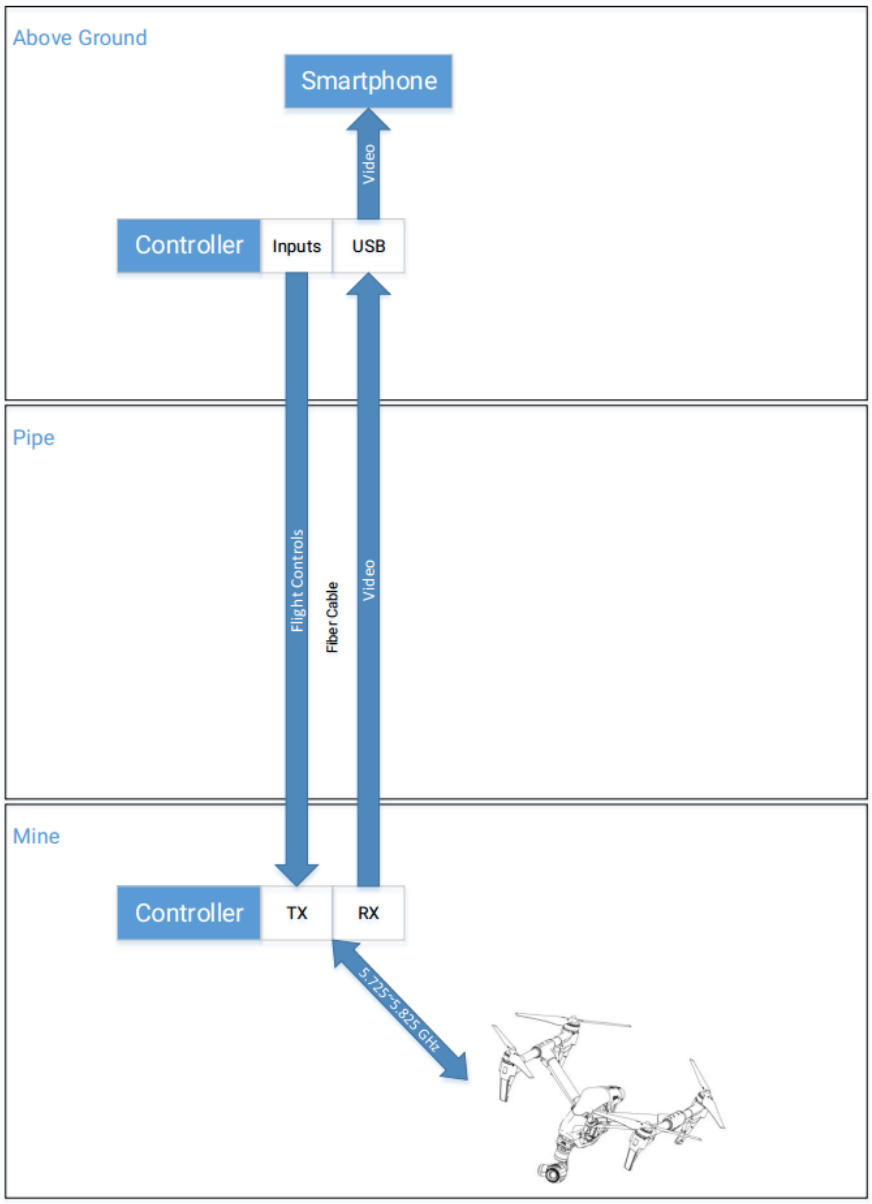

Figure 1.3: Overview of Fiber Optic Communication System

One solution involves the use of fiber optic cable to effectively transmit the radio signals from the surface into the mine through the borehole. An example of how such a fiber cable could be deployed down a borehole is seen in Figure 1.3. The joystick commands sent from the controller are interpreted and sent through the fiber link to a transmitter in the mine, which then sends the commands via RF to the UAV underground. The details of this type of system implemented on a commercial DJI quadcopter can be viewed in the Appendix, which also documents all parts used in the borehole demonstration.

The primary focus of this thesis is the automated spatial centering function of the UAV. Automated spatial centering would lessen the operational burden on the pilot by automating much of the collision avoidance. There are several commercially available flight controllers and quadcopters that have self-stabilizing hardware integrated into the platform. However, there is no readily available built-in distance sensing functionality which properly adjusts the quadcopter position to ensure equal distances from all surrounding surfaces in a confined space.

1.2 Hardware

1.2.1 LEDDAR Sensor

The light-emitting diode detection and ranging (LEDDAR) sensor is a unique technology developed by LeddarTech. It uses light emission from a set of six LED's to illuminate an area of interest, and the reflected light from the object is received by an on-board photodetector. It is the pulsing of the diffused light emission, the collection of the reflected light, and the s

ignal processing of the full waveform received that allows distance measurements to be made based on the light's time of flight[1].

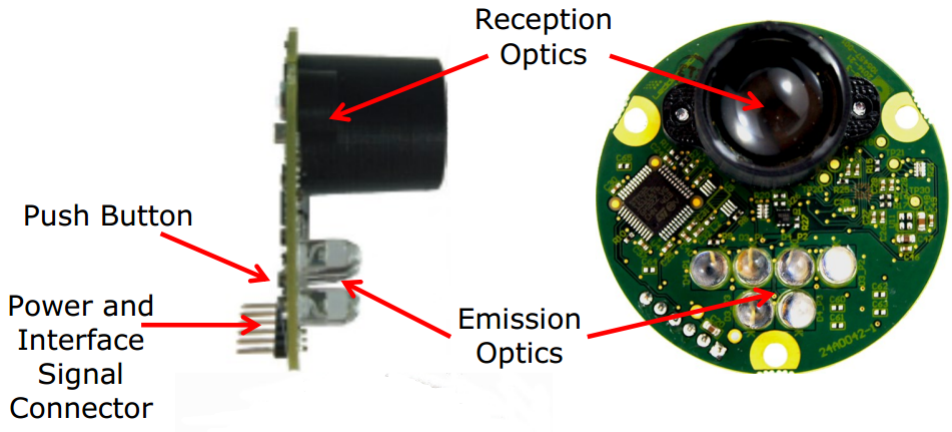

Figure 1.4: LEDDAR One Module [1]

The LeddarOne sensor operates on a 5.0 V power source and consumes a maximum of 1.3 W of power. It consists of an array of 6 LED's and a single photoreceptor with a 3°

conic beam. The backside of the sensor houses the interface and power pins for UART data transmission. Figure 1.4 shows the locations of these components on the board[1].

The LEDDAR sensor has a detection range of 0 m to 40 m. The maximum range is dependent on the reflectivity of the material on which the light is reflecting, where an object with a higher reflectivity will result in a larger maximum range close to 40 m. The worst case scenario in which the material has a low reflectivity results in a maximum range closer to 8 m. It has a stated accuracy of +/- 10 cm and a precision of 5 mm, which is one standard deviation from the measured distance. The data in table 1.1 below show the results of measurement tests conducted for 10 seconds each, where a matte white object was placed at various distance from the sensor. The actual distances at which the object was placed relative to the sensor are on the left-most column. The results mostly verify the specifications, though some of the distance errors were greater than the stated +/- 10 cm. However, the standard deviation results were excellent, and the precision of the sensor is more important than accuracy for this application.

Table 1.1: LEDDAR Test Data

	Measured Distance (cm)	**Error (%)**	**Standard Deviation**
0 cm	**7**	**7**	**0**
100 cm	**108.66**	**8.6**	**0.005**
200 cm	**215.45**	**7.7**	**0.005**
300 cm	**285**	**5.0**	**0**
400 cm	**401.78**	**0.45**	**0.004**

Due to the proprietary nature of the LEDDAROne sensor, certain technical details of the logic design are unavailable. However, the overall sensor architecture is shown in figure 1.5.

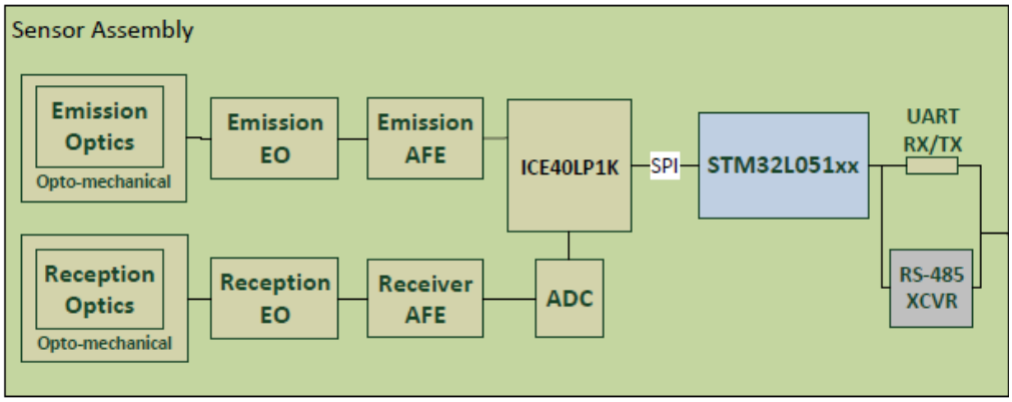

Figure 1.5: LEDDAR Sensor Architecture [1]

The major components of the sensor assembly are the emission and reception optics (LED's and photodetector), the STM microcontroller, and the ICE40LP1K FPGA. The LED's are used to generate the light pulses, which ultimately provide the sensor with distance data after the pulses are received by the photodetector.

Both the emission and reception optics are fed through AFE (Analog Front End) circuitry before being sent to the FPGA. This FPGA is used to control the LED pulse rate and the data acquisition timing of the receiver. It produces a set of waveforms based on the received light pulses, which is sent to the STM microcontroller. The STM microcontroller recovers these waveforms from the FPGA, and performs the full waveform analysis, producing the distance measurements sent over UART [1]. This full waveform analysis is explored in more detail in Figure 1.6.

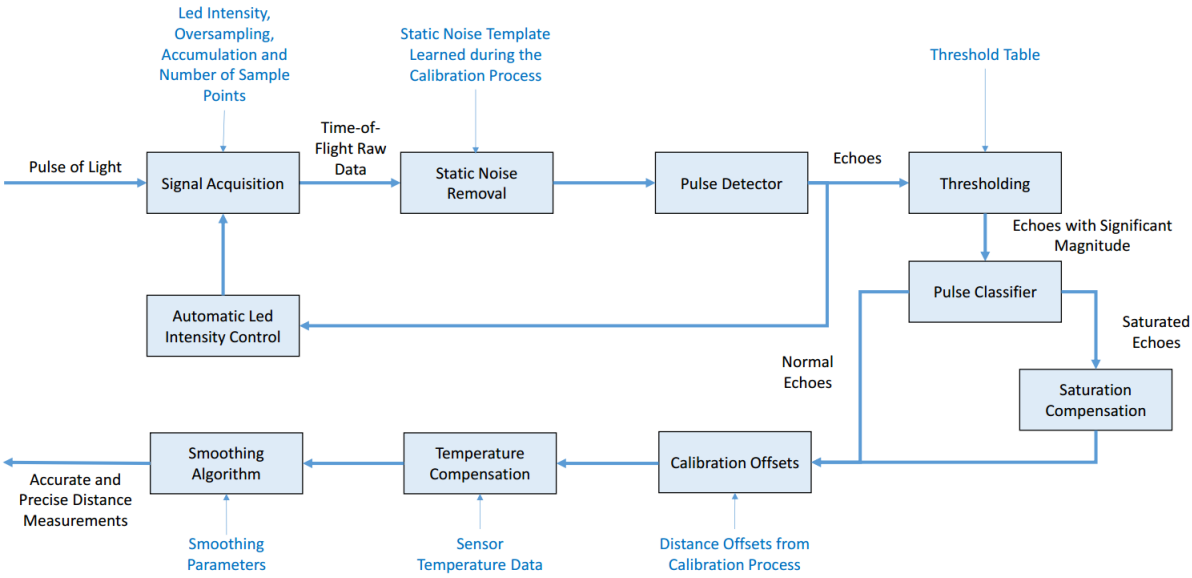

Figure 1.6: LEDDAR Signal Processing Algorithm [1]

Figure 1.6 shows the overview of the algorithm used by the LEDDAR sensing module to obtain distance measurements. The process begins with signal acquisition, in which the single photosensor on the sensor acculumates the received light pulses in such a way which produces a full-waveform signal. Once this signal is acquired for a given sampling interval, any static noise generated from external sources (electromagnetic interferences, sensor enclosure, etc.) is removed. This allows for much more accurate distance sensing.

Once the noise has been cleaned from the full-waveform signal, the pulses detected by the photoreceptor are analyzed. Due to the nature of the sensing platform, the photoreceptor can detect light reflections from more than a single object. This stage of the algorithm uses a modifiable amplitude threshold value to remove any detected pulses below this amplitude. This helps to minimize any discrepancies in the distance measurements of objects with differing reflectivity or smaller objects obscuring the primary object of interest. This stage also controls the intensity of the LED's based on the pulse analysis. If the pulses suddenly become saturated, or too weak, the intensity of the light emitted from the LED's can be adjusted in real time to maintain optimal measurement accuracy.

The LEDDAR sensor then determines which pulses in the full-waveform signal are saturated, and which are considered normal. A saturated pulse is generated when an object being

measured has high reflectivity or is too close to the sensor. The reflected light intensity can be so great that it will clip the full-waveform signal, which significantly impacts the distance measurement accuracy, especially at smaller ranges. This stage of the algorithm compensates for these over saturated pulses, providing distance measurement accuracy better than 10 cm.

After this stage, a temperature compensation scheme is applied, which attenuates the measured distances over a range of temperatures. Specifically, it is designed to stabilize the distance measurements to within 1 cm of accuracy in less than 10 seconds immediately after powering the sensor. It will also ensure distance accuracy over the specified operating range of -45°C to +85°C. This is an especially relevant step since the operating environment for the quadcopter has the potential for a variety of ambient temperatures (e.g. fire, cold air drafts).

The final stage of the algorithm is smoothing, which reduces measurement jitter. In this case, jitter can be viewed as the variability of received distance measurements. The smoothing algorithm continuously adapts the cutoff frequency as a function of the measurement noise. As a result, the standard deviation of the measurements is reduced, which produces a more stable and precise distance reading [1].

1.2.2 MODBUS Protocol

The LEDDAR sensor transmits data over a 3.3V UART link, utilizing the MODBUS protocol. The MODBUS protocol lies at the application layer, providing a client/server communication between two different devices. In the case of the quadcopter, the flight control board (client) interfaces with the LEDDAR sensor (server). It uses big endian encoding, meaning that the most significant byte is sent first.

The overall premise of the protocol relies on sending specific 1 byte function codes from the client to the server to perform various tasks (i.e. reading registers, setting registers, etc.). Valid function codes range from 1 to 255, and are usually followed by a data request field. This data field is used for information relevant to the function code being used, such as register addresses, the number of data bytes in the field, and the number of data items to be handled by the request [5]. The transaction is fairly straightforward, and is initiated by the client (flight control board) sending this function code and data request over the 3.3V UART connection to the server (LEDDAR Sensor). The server then returns the same function code with the data response appended. This process is illustrated in Figure 1.7.

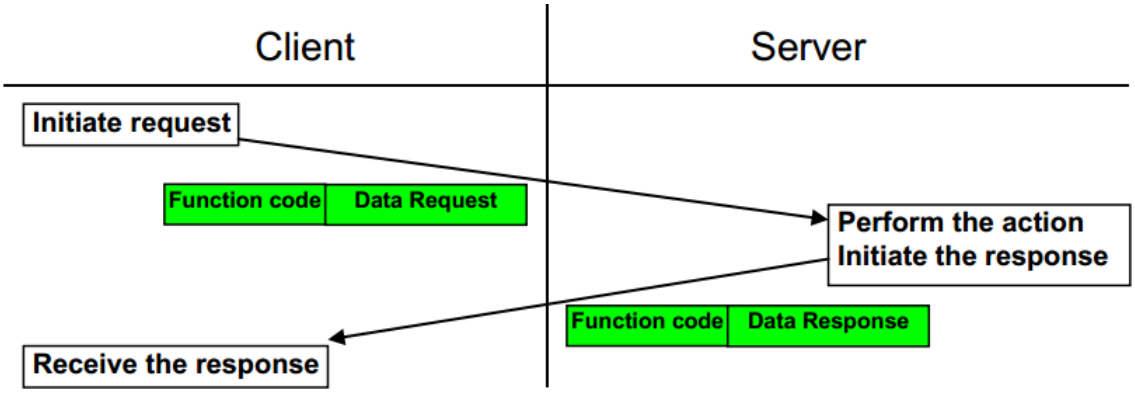

Figure 1.7: MODBUS Transaction [5]

For the purposes of this research, the function code of interest is the Read Input Register code (0x04). A typical 0x04 read request adheres to the following request/response pair [5]:

Request

Function code	1 Byte	**0x04**
Starting Address	2 Bytes	0x0000 to 0xFFFF
Quantity of Input Registers	2 Bytes	0x0001 to 0x007D

Response

Function code	1 Byte	**0x04**
Byte count	1 Byte	2 x **N***
Input Registers	**N*** x 2 Bytes	

***N** = Quantity of Input Registers

Figure 1.8: Read Input Registers (0x04) [5]

The input registers on the LEDDAR One sensor module are implemented in a specific way. There are 10 registers used, ranging from decimal memory addresses 20 to 29, which contain the measured amplitudes of multiple detections, as well as the timestamp, temperature readings, and more. The figure below illustrates the way in which the registers are implemented in the LEDDAR sensor [1]:

Address	Description
20	Least significant 16 bits of timestamp.
21	Most significant 16 bits of timestamp.
22	Temperature in 1/256th of a Celsius
23	Number of detections
24	Distance in millimeters of first detection
25	Amplitude of first detection
26	Distance in millimeters of second detection
27	Amplitude of second detection
28	Distance in millimeters of third detection
29	Amplitude of third detection

Figure 1.9: LEDDAR MODBUS Registers (Decimal Addressing) [1]

By leveraging the MODBUS protocol and the information in Figure 1.9, it is possible to construct a MODBUS request message to obtain measurement readings from the LEDDAR sensor. Based on the MODBUS protocol, a read register request begins with a MODBUS address (default of 1), followed by the format specified in Figure 1.8.

	Modbus Address	Function Code	Starting Address	Quantity of Input Registers (10)
Hex	01	04	00 14	00 0a
Dec	1	4	20	10

Figure 1.10: MODBUS Read Register Bytes

This message is sent over the 3.3V UART link from the flight control board to the LEDDAR module. Note that the addressing uses hexadecimal values (e.g. starting address 0x00 0x14 represents 20). Referring back to the MODBUS request/response protocol for a register read in Figure 1.8, the response from the LEDDAR sensor will look like the following sample, utilizing big endian formatting:

				Input Registers					
	Modbus Address	Function Code	Byte Count	20	21	22	23	24	25
				Time(LSB)	Time(MSB)	Temperature	Detections	Distance	Amplitude
Hex	01	04	14	BFBB	002D	26E6	0001	0BA0	0F43
Values of interest						**38.9 °C**	1	**2.976m**	

Figure 1.11: MODBUS Read Register Response

It should be noted that registers 26-29 are 0 since the LEDDAR sensor is configured to obtain only a single measurement, verified by the value of input register 23. It should also be noted that the timestamp value in registers 20 and 21 represent the total time in milliseconds since the LEDDAR sensor was booted. The temperature value in Celsius is obtained by converting the big-endian hexadecimal to decimal, and dividing by 256. The distance value is obtained by converting the value of register 24 to decimal, which provides the distance measured in millimeters. This demonstrates that the primary value of interest for the quadcopter centering application is obtainable by using the MODBUS request/response protocol [1].

1.3 Flight Controller

The flight control board functions as the primary computational core of the quadcopter system. It provides outputs to the electronic speed controllers (ESC) which control the motor speeds, receives transmitted RF signals from the radio controller, interfaces with the LEDDAR sensor, and computes a variety of other flight-related calculations like the PID control system.

An SPRacingF3 flight control board was used due to its tight integration with the cleanflight software and the availability of multiple UART connectors. The board was designed and produced by the primary contributor of cleanflight, so it also works well as a development platform for new versions of the cleanflight software. An image of the flight controller used can be seen in Figure 1.12.

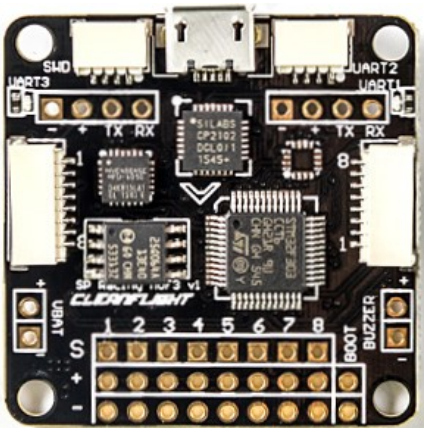

Figure 1.12: SPRacingF3 Flight Control Board [6]

The SPRacingF3 relies on the STM32F303 microprocessor running at 72 MHz as its primary computational core. It also has the ability to process PID calculations faster due to a dedicated Floating Point Unit (FPU) co-processor. A board integrated MPU6050 accelerometer/gyro sensor is used for flight stability and sensor feedback for the PID Controller. There is support for up to eight motor connections, though only four are used for the quadcopter.

1.4 Cleanflight Process Flow

Cleanflight was chosen as the flight control software due to its open source nature and available documentation. It has a wide range of supported platforms, including the SPRacingF3 flight control board (FCB) used. Configuration of the software is performed primarily through the use of a computer application which communicates over USB to the FCB. The block diagram in Figure 1.13 shows the overall process flow of the cleanflight software as it operates with the LEDDAR task inserted.

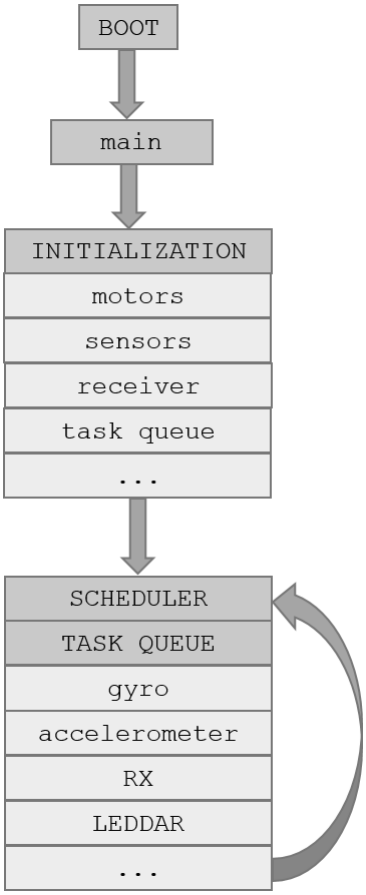

Figure 1.13: Cleanflight Process Overview

The overall process of Cleanflight is fairly straightforward. On system boot, various system elements are initialized, including the motor operations, sensor port connections or specific configurations, and the instantiation of the tasks queue. The scheduler function loops indefinitely, stepping through the tasks that were defined during the initialization

stage. Each one of these tasks performs specific operations, including flight stabilization (PID control), receiver information, and sensor updates.

Chapter 2

Literature Review

This chapter presents the related work to quadcopter control schemes, sensing systems, and collision avoidance.

2.1 Quadcopter Flight Dynamics

As with any flight platform, the possible range of motion is critical to understanding flight performance and stability. Figure 2.1 illustrates the 6 degrees of freedom for a quadrotor aircraft, as seen from two different views. The rotational movement about the x-y plane in 2.1(a) is referred to as "yaw," the rotational movements in 2.1(b) are called "roll" and "pitch", and the vertical movement in 2.1(b) labelled z is called "throttle." These four movements encompass the normal operation of the quadcopter from a remote controller, where the two joysticks are able to move in four total directions. The remaining two degrees of freedom, x and y in 2.1(a), are described as the total forward and side to side movement of the quadcopter as a result of roll/pitch change or external forces like air turbulence[7].

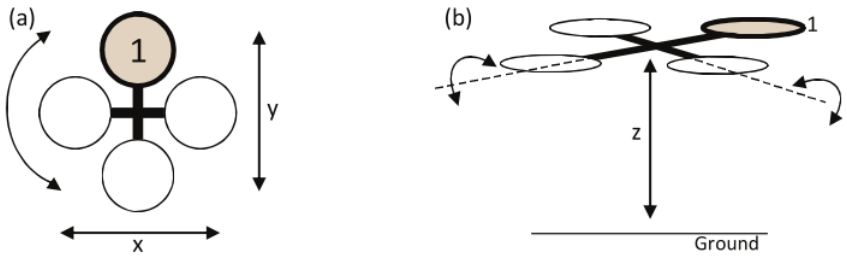

Figure 2.1: Six degrees of freedom of the quadcopter from (a) top-down (b) frontal view [7]

2.1.1 Motor Orientation

As with any rotating motor, there is a torque produced. In order to ensure stable control of the quadcopter, the rotational movements of the four motors must be correctly oriented so that the total net torque is zero. Otherwise, the quadcopter will not hover in a stable position, and will produce a strong yaw rotation. Another flight platform that encounters this issue is a helicopter, where a secondary vertical propeller is used to cancel out the torque that would otherwise cause the aircraft to spin uncontrollably. Essentially, if all four propellers on the quadcopter were configured to spin in the same direction, Newton's third law of motion (for every action there is an equal and opposite reaction) would cause the quadcopter to spin in the opposite rotation from the propellers [8]. Thus, it is important to configure the motors in pairs, operating in clockwise and counterclockwise rotations as illustrated in 2.2.

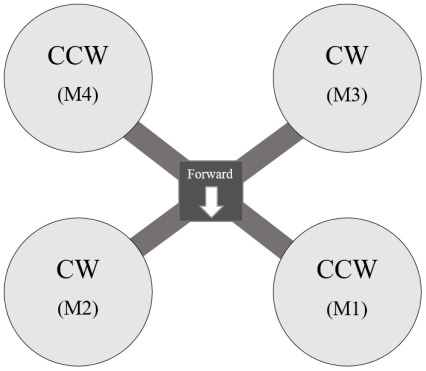

Figure 2.2: Propeller spin configuration for zero net torque [8]

Each of the four motors above is identified by a motor number (M1-M4). By varying the speeds of each of the motors different control actions can be accomplished. For throttle adjustments, the motor speeds for all four motors are the same, resulting in a direct upwards ascent or descent.

For pitch adjustments (forward or backwards movement), an offset speed is subtracted from M1 and M2, and added to M3 and M4. The increased thrust of the rear propellers combined with the decreased thrust of the front propellers causes the quadcopter to move forward. The same applies for a reverse movement, in which the offset addition and subtractions are flipped.

For yaw adjustments (horizontal rotation), an offset speed is subtracted from M2 and M3, and added to M1 and M4. This results in a counterclockwise rotation since there is no longer a net zero torque due to the increased motor speed of the CCW propeller pair compared to the CW pair. A similar offset can be applied for a clockwise rotation by increasing M2/M3 and decreasing M1/M4.

For roll adjustments (side-to-side), an offset speed is subtracted from M2 and M4, and added to M1 and M3. This results in an increased thrust from the right side, which causes the quadcopter to roll to the left. The same approach is used for rolling to the right, in which M2/M4 have increased speed offsets relative to M1/M3.

It should also be noted that for the pitch, yaw, and roll adjustments there is no change in altitude. Since the offset speed is added and subtracted in pairs, there is no net upwards or downwards thrust. Alterations in the motor speeds are more commonly affected by various combinations of throttle, yaw, pitch, and roll. The job of the flight control unit is to interpret the commands sent from the joysticks on the remote controller and adjust the motor speeds accordingly. In order to add stability and increased control to the quadcopter, a closed loop feedback system is used [8].

2.1.2 The PID Controller

A Proportional-Integral-Derivative (PID) controller is a three part feedback control system that is used to tune a closed loop system. In the case of a quadcopter, a properly set PID controller can enhance the responsiveness and stability of the platform.

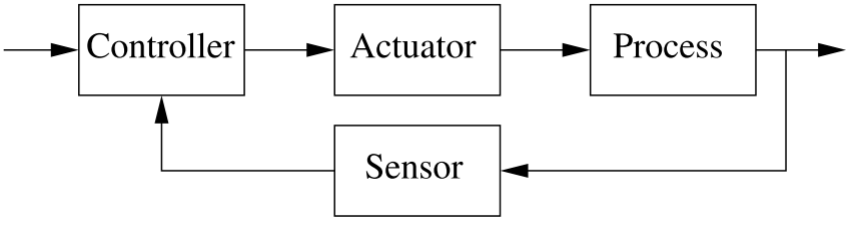

Figure 2.3: Feedback Control Loop [9]

The PID controller relies on the basic structure of a typical high level feedback control loop as seen in Figure 2.3. A reference signal is sent to the controller, which in the case of

a quadcopter is the flight control board. This then forwards the received joystick command to the actuators, which are ultimately the motors powering the propellers. The alteration in motor speed occurs in the process block, and sensor data collected from the gyroscope is used as feedback to the controller. This results in a closed loop system in which the current rotational state of the quadcopter is used as a feedback method to control the speed commands sent to the motors [9].

In the PID controller, a parallel approach is used to incorporate the proportional, integral, and derivative corrections. An overview of this type of system is shown in Figure 2.4.

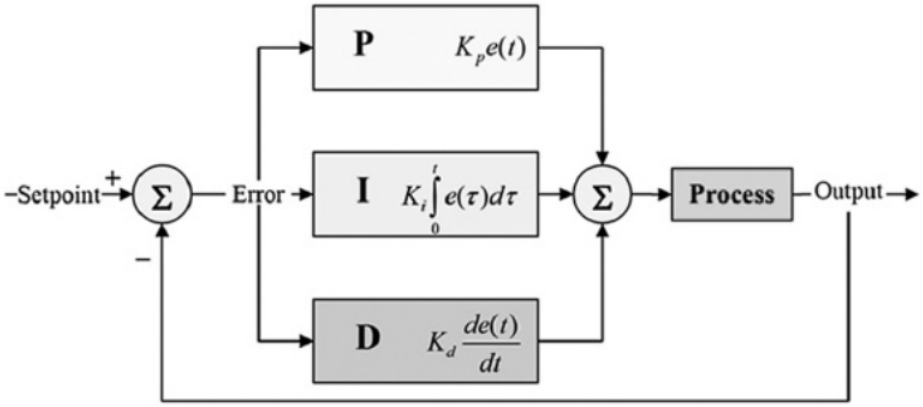

Figure 2.4: PID Block Diagram [8]

The setpoint (the input to the system) can be interpreted as the command that is sent from the joystick to the FCU at a given time t. For instance, if a pitch forward command is issued by moving the right joystick forward by a certain amount, a specific setpoint is associated with that joystick movement. The error used in the P, I, and D blocks can be described as the difference between the output and the setpoint as a function of time ($e(t)$). For instance, if the quadcopter is level and a pitch forward command is suddenly issued from the joystick, $e(t)$ will be very high for the first few values of t since the output is smaller than the setpoint. As the angle of the quadcopter reaches the desired setpoint based on the throttles of the motor pair pushing it forward (as described in 2.1.1), $e(t)$ will begin to decrease. However, if the joystick is suddenly released back to center, resulting in a desired setpoint of 0, $e(t)$ will once again return to a large value until the quadcopter returns to a horizontal position and the output matches the setpoint [8].

The summed output from the corrections provided by the parallel adjustments in the P, I, and D blocks can be described by equation 2.1. It should be noted that the PID controller is applied to each axes, which include pitch, roll, and yaw motion.

$$K_p e(t) + K_i \int_0^t e(\tau)d\tau + K_d \frac{de(t)}{dt} \tag{2.1}$$

The Proportional Block

The proportional (P) block responds to the current control error and is described by equation 2.2, where K_p is the proportional gain and $e(t)$ is the error signal as a function of time:

$$K_p e(t) \tag{2.2}$$

This is perhaps the most important part of the PID system, since it responds directly to the current changes in quadcopter orientation provided by the gyroscope. In other words, it is directly proportional to the current control error at the present time t [8]. The value of the proportional gain K_p determines the strength of the correction applied. Relying only on the proportional correction could lead to some potential issues, such as overcompensation. For instance, if a quadcopter has been traveling forward and the joystick is released back to center position (no more forward movement is desired), the proportional corrections made to the throttles may over correct past the stable state. This means that the quadcopter could get stuck in an oscillating state where it never fully stabilizes since it is constantly trying to correct its orientation based on the present values. This can be partially solved with the addition of the integral block [9].

The Integral Block

The integral (I) block relies on the summation of the error over time and is described by equation 2.3, where K_i is the integral gain and $\int_0^t e(\tau)d\tau$ is the additive summation of the error signal over the given time period t:

$$K_i \int_0^t e(\tau)d\tau \tag{2.3}$$

Since the integration of the error function results in a cumulative sum of the the values of the errors over the recent time t, it reacts much more slowly than the proportional adjustments. The goal of the integral block is to adjust the steady state value to zero over the time period t. This is especially relevant in the scenario where the quadcopter does not fully adjust to the horizontal position and maintains a slight angle, causing it to drift from center. If there was only a proportional adjustment in play, the feedback would not be strong enough since the error would be a relatively small value. With the addition of the integral block, over time the small values of $e(t)$ accumulate to a more significant total value, and the quadcopter can eventually be returned to the horizontal position. The value of the integral gain K_i determines how much influence this adjustment has on the overall control, and is generally kept smaller than the proportional gain [8].

The Derivative Block

The derivative block (D) relies upon the predicted changes in the error function, and provides a rapid response to the error signal. It can be described by equation 2.4, where K_d is the derivative gain and $\frac{de(t)}{dt}$ is derivative of the error as a function of time.

$$K_d \frac{de(t)}{dt} \tag{2.4}$$

The derivative of the error function in a given time slice Δt provides information about the current trend of the value of $e(t)$. This means that future error values can be predicted based on the current progression of $e(t)$. It is possible to predict an over-correction caused by the proportional adjustment, thereby compensating for the overshoot and causing the quadcopter to stop closer to the horizontal position. For instance, if a pitch forward command is issued by moving the joystick from the center position, $e(t)$ will have a decreasing trend as the output grows closer to the setpoint value. This results in a negative adjustment from the derivative block. If the quadcopter has been traveling forward and the joystick is released, the derivative block will provide a strong positive value since the trend of the error $e(t)$ is

increasing back towards 0. The value of the derivative gain K_d determines the strength of this adjustment, and is usually kept relatively small. It should also be noted that the value of Δt is minimized to prevent erroneous derivative calculations due to sensor noise [8].

2.2 Related Quadcopter Sensing and Applications

There are a large variety of ways in which autonomy is implemented on quadcopters, many of which rely on features that only work well above ground. Some of the most common sensors used for self stabilization and altitude control are barometers and GPS positioning systems. Since GPS signals cannot penetrate the ground, GPS cannot be used in an underground mine.

2.2.1 Ultrasonic Sonar Sensor

Figure 2.5: PING)))^{TM} Ultrasonic Distance Sensor [2]

Perhaps the most ubiquitous and low cost distance sensor used on a robotics platform is the ultrasound sonar sensor. One such sensor is developed by Parallax Inc, and uses the time of travel of sound pulses as a way to determine distance, much like echolocation [7].

The communication protocol illustrated in Figure 2.6 relies on the transmission of a short ultrasonic burst, and the return time of the burst from the target of interest. A 5 μs pulse, referred to as the "trigger" pulse (t_{out}), is generated by the microcontroller host and transmitted on the SIG pin. This causes the PING sensor to transmit a 40kHz burst for 200 μs (t_{burst}). The burst travels through the air, bounces off a target in its path, and then returns to the sensor. Meanwhile, a 5V pulse is produced by the sensor on the SIG pin after a set hold off time of 750 μs, and the pulse ends once the reflected burst is heard by the sensor. The width of this pulse (t_{in}) corresponds to the distance from the sensor to the target, and can range anywhere from 115 μs to 18.5 ms [2].

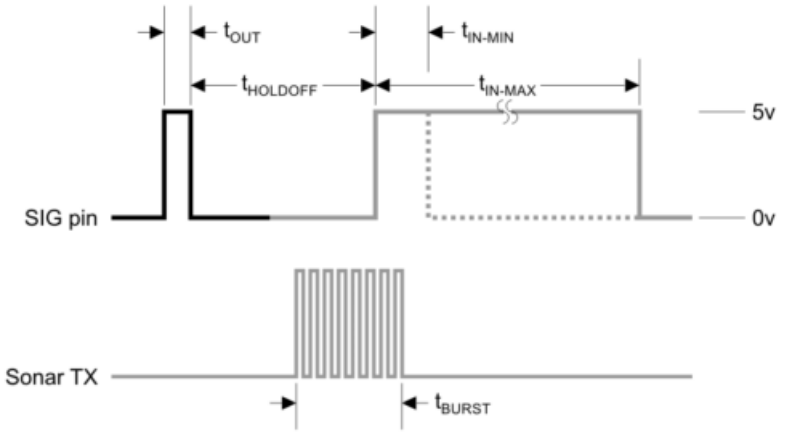

Figure 2.6: Ultrasonic Distance Sensor Communication Protocol [2]

The main limitations of this sensor are the detectable distances, angle of detection, and size of the detected object. The maximum measurable distance is around 3 m, and the angle between the object being detected and the sensor must be less than 45° [2].

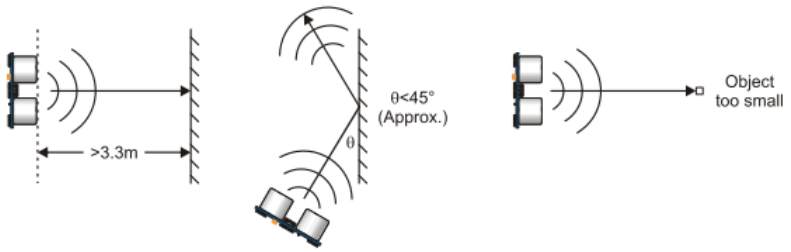

Figure 2.7: Sensor Limitations [2]

Autonomous Flying Cameraman

One application that has previously been researched is the use of a quadcopter as a cameraman, which automatically moves to a person's position based on the location of colored markers attached to a microphone. Since the quadcopter must operate within close proximity to a person, obstacle avoidance is an important consideration. The research team first attempted to use multiple ultrasound sonar sensors to detect any obstacles located on the sides of the quadcopter, for a total of four sensors arranged as seen in Figure 2.8 [10].

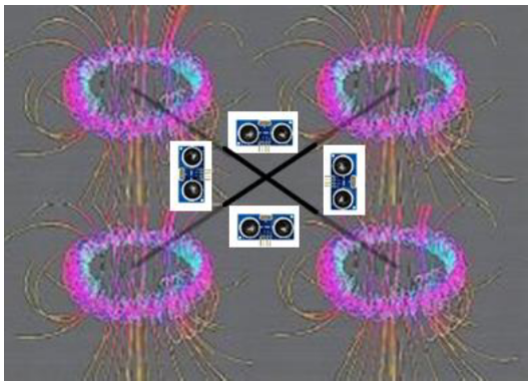

Figure 2.8: Sonar Sensors for Obstacle Avoidance [10]

The most common problem with using ultrasonic sensors on a quadcopter is noise caused by air turbulence produced by the propellers interfering with the sensor accuracy. This effect is commonly referred to as "prop wash." This effect can be observed in Figure 2.8, in which the air flow lines produced by each of the four propellers are illustrated. In addition to the air turbulence produced, the significant sound of the spinning propellers can cause erroneous distance readings from the sonar sensors [17]. Based on these considerations, it was determined that the use of a depth sensor that is not sound-based was the best approach. IR-based distance sensors (SHARP GP2D12) were then used instead, since the IR signal is not affected by air turbulence or sound. These sensors have an effective range of about 80 cm [10].

2.2.2 LIDAR

LIDAR (LIght Detection and Ranging) sensors are commonly used as a means to obtain a high-resolution distance measurement. They utilize the time of flight of light between the laser source and the object being detected, similar in some ways to the ultrasonic sensor except at a much faster rate and with a different medium [11].

There are many different ways to measure the time it takes for a light pulse to reflect off an object, but a common approach uses a capacitor as a timing device, as seen in Figure 2.9.

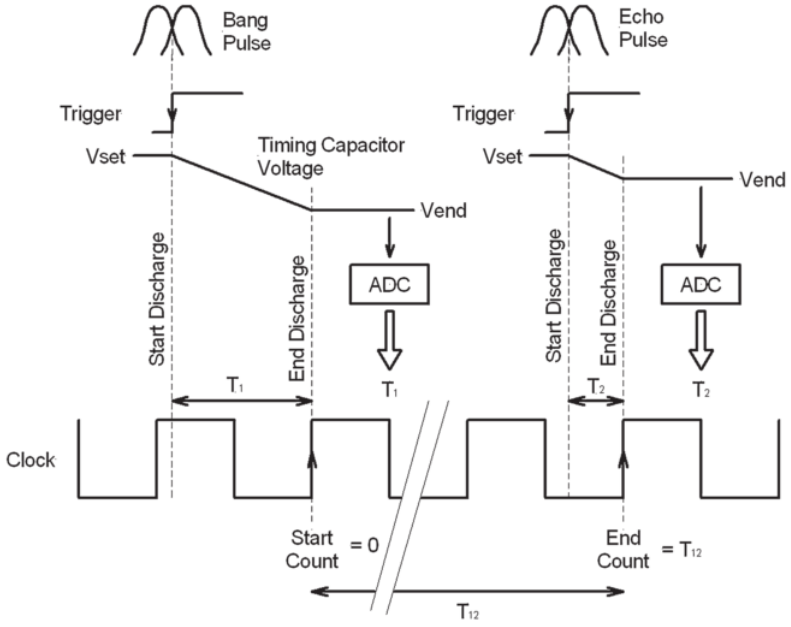

Figure 2.9: LIDAR time-to-digital conversion (time of flight) [11]

In a typical LIDAR system, there is a synchronous and asynchronous component. In Figure 2.9, a system clock of around 500 MHz is used to measure the synchronous portion, and the capacitor is used for the asynchronous timing of the laser pulse. The "Bang Pulse" creates a trigger which starts the discharge of the capacitor voltage, and the system clock is used to stop the discharge. The capacitor acts as a time-to-amplitude converter (TAC). It uses a known value of V_{set} at the beginning of the bang pulse so that it can use the value of the capacitor voltage V_{end} at the rising edge of the next clock cycle to represent the time elapsed. An analog to digital converter (ADC) converts this voltage to a time value T_1,

which represents the time at which the bang pulse was transmitted.

The approach used for determining T_1 is also applied to the reception of the echo pulse, which is the reflected light from the object being sensed. A trigger is generated when the echo pulse is received on the light-receptor, and the discharge of the capacitor is used in conjunction with the system clock and ADC to generate a time value T_2. This represents the time at which the reflected light pulse was received. The time of flight can then be determined by comparing the difference T_{12} with the number of system clock cycles elapsed [11].

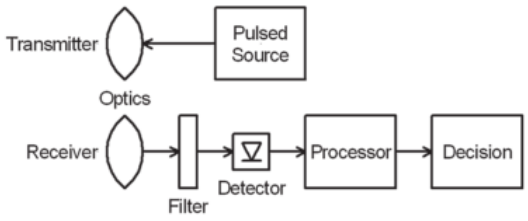

Figure 2.10: Typical LIDAR System Overview [11]

A typical LIDAR system using direct detection can be seen in 2.10. As with most distance sensors, it consists of a pulsed source and a receptor. In the case of LIDAR sensors, the pulsed source is light-based (usually laser) and travels through transmission and reception optics. The reflected light pulse received through the reception optics is then filtered depending on noise conditions, and a photodiode detector registers the light [11].

Aerial Three-Dimensional Mapping

A common application for LIDAR sensors is the precise 3D mapping of environments. Due to the aerial nature of the quadcopter platform and the precision of the LIDAR sensor, it is quite common to use them for surveying purposes in a variety of applications. These applications includes accurately mapping streets, tunnels, mines, caves, forests, and more. Since conventional terrain mapping involves the use of a manned craft flying at a high altitude with a downward facing sensor, the resulting point clouds are relatively sparse and lack detail. By mounting a lightweight 2-D laser scanner on the bottom of a quadcopter, it is possible to obtain a much denser point cloud map of the environment. This data is often used for autonomous navigation, commonly referred to as Simultaneous Localization and Mapping (SLAM) [12].

Figure 2.11: Passive rotation of 2-D Laser Scanner [12]

One previous research project mounted a 2-D laser scanner underneath the quadcopter, and the air turbulence produced by the propellers caused the sensor to passively rotate. The laser scanner used was a Hokuyo UTM-30LX-F, which has a 270° field of view and a 100 Hz scan rate. The quadcopter with the sensor system attached can be seen in Figure 2.11.

Since an accurate point mapping of the craft's environment is produced, it is possible to operate the quadcopter with confidence in GPS-deprived environments. A continuous-time mapping approach was used, in which the trajectory of the sensor payload was estimated from the range measurements and inertial measurements from a secondary sensor. The trajectory in this case can be described as the continuous time function that defines the orientation of the quadcopter within the six degrees of freedom as described in Figure 2.1.

With this information known, a 3D point cloud map can be produced by plotting the data points produced from the laser scanner onto a coordinate system [12].

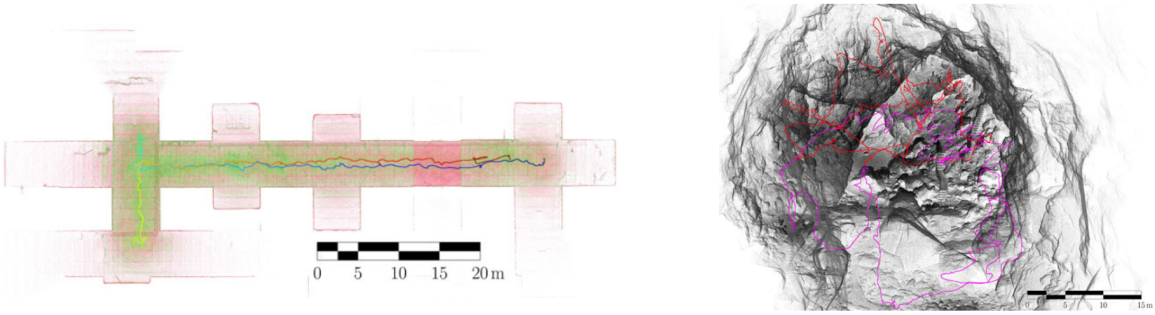

(a) Overhead View of a Mine Entry

(b) Cave

Figure 2.12: Point Cloud Results in Different Underground Environments [12]

The point clouds produced by the platform produced accurate representations of the surrounding environment in a variety of applications. Two such examples that are particularly relevant to an underground mine scenario can be seen in Figure 2.12. For the mine entry scenario shown in 2.12a, the colored lines represent the trajectory information a t a given point in time, from blue to red. Only a single pass was required to properly map the mine entry. The point cloud produced in 2.12b was the result of two separate datasets, and are indicated by the red and purple lines [12].

2.2.3 Inertial Measurement Unit

Perhaps the most critical component of a quadcopter control system is the inertial measurement unit (IMU). This sensor consists of motion detection elements, and uses a gyroscope to determine the angular rate and an accelerometer to detect the acceleration of the quadcopter. Inertial Measurement Units found on flight control boards are classified as MEMS (Micro-Electromechanical Systems) devices, which are small three dimensional structures produced on a silicon substrate through the use of various chemical processes. [13].

Gyroscope

The operating principles of a typical MEMS gyroscope rely on a "tuning fork" structure as seen in Figure 2.13.

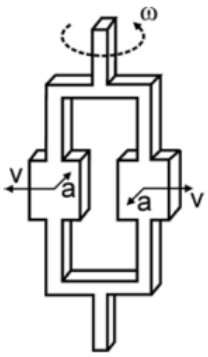

Figure 2.13: Operating Principle of MEMS Gyroscope [13]

This structure relies on the oscillation of the two masses m in the center of each fork as the object rotates about ω. The rotation generates a force described in equation 2.5, where a is the acceleration of the mass, ω is the angular rage, and v is the mass velocity:

$$F = ma = -2m(w \times v) \tag{2.5}$$

The displacement of the masses during rotation is sensed with a capacitive comb structure, where the displacement corresponds to an angular rate. This type of MEMS structure can be used to detect the angular changes for both the pitch and roll directions of the quadcopter [13].

Accelerometer

Accelerometers implemented as a MEMS device rely on the displacement of a mass m. The inertial force acting on the mass when the sensor is moved results in a force similar to a spring reaction with a spring constant K. A small amount of dampening D is applied to the system, and the displacement x of the mass m results in a proportional relationship between the acceleration a and displacement x. A diagram illustrating this effect can be seen in Figure 2.14.

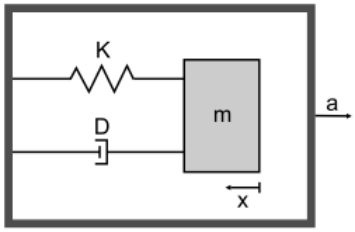

Figure 2.14: Operating Principle of MEMS Accelerometer [13]

A common implementation of a MEMS accelerometer uses multiple suspended masses with capacitive plate pairs directly above. This configuration can be seen in Figure 2.15.

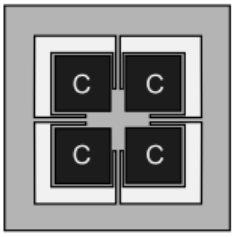

Figure 2.15: Top view of a tri-axial accelerometer [13]

A single suspended mass is used in conjunction with four capacitors arranged in a grid. When the sensor is stationary and there is no exposure to acceleration, the distance between the capacitor plates are all equal. This neutral position is illustrated in the middle section of Figure 2.16.

$$\Delta V = \frac{Q}{\Delta C} \approx \frac{Q\Delta d}{\epsilon A} \tag{2.6}$$

The relationship between the voltage and distance between the plates can be seen in equation 2.6, where Q is the electric charge, ΔC is the change in capacitance, Δd is the change in distance between the plates, ϵ is the dielectric constant, and A is the capacitive plate area [13].

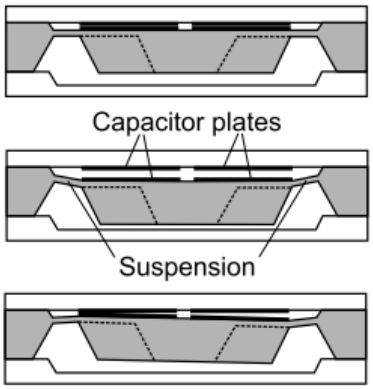

Figure 2.16: Side view of a tri-axial accelerometer [13]

The movement of the suspended mass causes the distances between the capacitive plates (Δd) to change. As a result of this motion, the voltage (ΔV) for each of the four capacitors is representative of the sensor motion. By comparing the different voltages of each capacitor, the direction and strength of the mass movement can be measured and meaningful data about the motion of the sensor can be calculated [13].

When the sensor is accelerated vertically, the distance between all four capacitors changes at the same rate due to the uniform motion of the suspended mass. This scenario is illustrated in the top section of Figure 2.16. If the sensor is moved horizontally, the mass causes the distance between the grid of capacitors to change depending on the direction in which the sensor was moved. For instance, the effect of a rightward movement on the mass and its affect on the distance between the capacitive plates can be seen in the bottom section of Figure 2.16. This approach can be used to detect horizontal accelerations in any combination of directions by comparing the different voltages corresponding to each of the spatial capacitors [13].

Vision-controlled Micro Air Vehicles

A European Union funded project called the "Swarm of Micro Flying Robots (SFLY)" was tasked with the development of a swarm of vision-controlled micro air vehicles (MAVS) to operate in GPS-deprived environments. The goal of the project was to enable autonomous navigation using a single on-board camera and inertial sensor data from the IMU [14].

One of the most common issues related to indoor position holding is drift. Even with the data from the IMU, the aerial nature of the platform and sensor inaccuracy and noise can cause the position of the craft to change over time. For the SFLY project, a combination of the IMU readings and the image processing analysis of the on-board camera was used to stabilize each of the three crafts and minimize positional drift. This so called "local navigation" module was run on-board, and used the data from the IMU to estimate the scale of the images produced by the camera.

Compared to other projects, this approach required a significant amount of processing power due to the image processing and sensor fusion used. An Extended Filter (EKF) framework was used to fuse the inertial measurements from the IMU with the camera output. A 24-element state vector X seen below describes the current state of the quadcopter based on this fused result [14]:

$$X = \{p_w^{i^T}\ v_w^{i^T}\ q_w^{i^T}\ b_\omega^T\ b_a^T\ \lambda\ p_i^s\ q_i^s\} \tag{2.7}$$

Where:
$p_w^{i^T}$ = position of the IMU
$v_w^{i^T}$ = velocity of the IMU
$q_w^{i^T}$ = attitude quaternion (3D complex equation) of the IMU
b_ω^T = gyroscope bias
b_a^T = accelerometer bias
λ = scale factor
p_i^s = relative position between the IMU and the camera frames
q_i^s = relative rotation between the IMU and the camera frames

A visual-odometry algorithm was used in conjunction with this fused state algorithm X to determine the position and orientation of the quadcopter at a given point in time. This approach resulted in an overall positional drift of about 1.5 meters in a 350 meter long trajectory test as shown in Figure 2.17 [14].

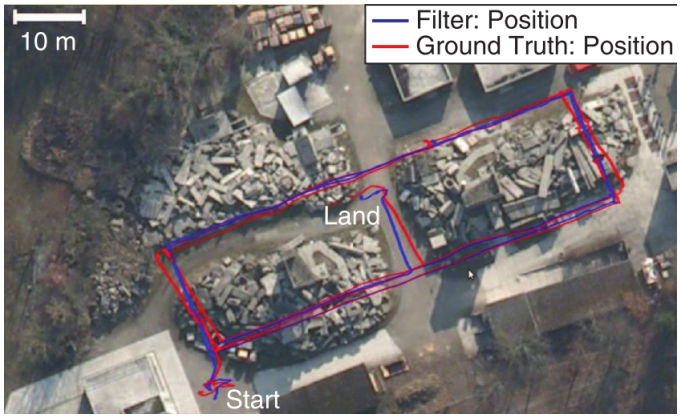

Figure 2.17: Vision Based Navigation using the camera-based position estimation. [14]

The blue line labeled "Filter" represents the positional data provided by the fusion of the IMU and camera, while the red line labeled "Ground Truth" is position data provided by GPS [14].

2.2.4 Summary

It can be clearly seen that the quadcopter platform provides the opportunity to integrate a variety of different sensing technologies. All of the sensor applications covered in this section are implemented so that the quadcopter can gain some sense of perception of its surroundings. The most commonly used sensor in commercial quadcopter flight control boards is the IMU, since the rotational and acceleration data is needed as inputs to the PID controller for flight stability. Cameras are also common in commercial quadcopters, though they are rarely used for navigation.

Cleanflight has the capability to support the ultrasonic sonar sensor natively, assuming the required I/O capabilities are present on the flight control board. The IMU is also used in cleanflight for PID calculations, flight stability, and flight control.

Table 2.1 below provides a summary of the sensors, including the LEDDAR sensor used on the test quadcopter.

Table 2.1: Sensor Comparison [1][2][3]

	Range (m)	**Pros**	**Cons**
PING)))™ Sonar	**0.02 - 3**	**Low Cost** **Commonly Used**	**Limited Range** **Subject to interference**
Hokuyo LIDAR	**0.1 - 60**	**Long Range** **High Accuracy** **Wide Range (270°)**	**High cost** **Weight** **Power consumption**
LEDDAR	**0 - 40**	**Moderate Cost** **Long Range** **High Precision**	**Accuracy** **MODBUS Overhead**

Chapter 3

Position Holding

3.1 Sensor Integration

In order to successfully implement and test the LEDDAR sensors, it is vital that accurate and timely sensor data is read into the Cleanflight software. This is accomplished through the use of UART ports on the Flight Control Board (FCB), which transmit and receive data to and from the LEDDAR sensors. Essentially, there must be some type of variable that exists within the Cleanflight construct that will consistently update based on the LEDDAR sensor distance readings. This is accomplished through the use of the tasking framework and the Input/Output (I/O) functionality in Cleanflight.

Due to cost and testing simplicity, two LEDDAR sensors are mounted on the quadcopter frame, with each using a separate UART port on the FCB. One is oriented to obtain distance measurements directly below the quadcopter, and the other is oriented to measure the distance between the center of the craft and obstacles to the right. The hardware used for implementation and testing can be seen in Figure 3.1.

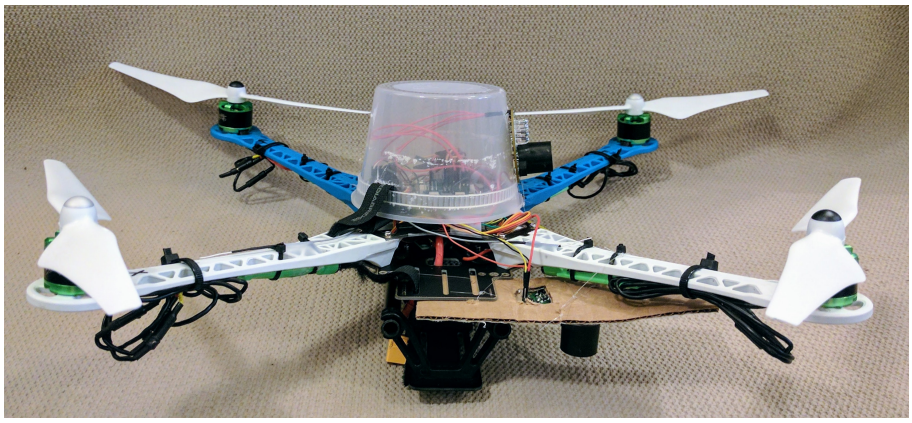

Figure 3.1: Quadcopter Platform

In order for custom code to be executed within Cleanflight, a task must be established in the task queue. This task contains many elements common to a scheduler, including priority, desired frequency of execution, and the task name. In order to receive measurements from the LEDDAR sensors, a specific sequence of bytes must be sent as described in section 1.2.2. Also, the data that is sent from the LEDDAR sensors to the FCB must be received and processed. This means that within the LEDDAR task, two UART ports are opened, data is transmitted to the sensors, and finally data is read from the UART ports. This effectively results in consistent distance readings of height above ground level and distance to obstacles on the right side of the quadcopter. Safeguards are implemented to ensure that data is only read from the UART ports when there are bytes waiting in the receive buffer. This means that even if a sensor is disconnected or stops functioning, the flight controller will not enter an unknown state and cease functioning.

Once data is acquired from both sensors, additional processing must be completed to control the altitude and attitude of the quadcopter in response to the measured distances. Both the altitude hold and wall avoidance algorithms employ an additional PID control system which appropriately adjusts the RC commands to maintain a set distance.

3.2 Linearized Mathematical Model of a Quadcopter

The functioning of a quadcopter in flight can be described by mathematical models which define its kinematics and dynamics [15]. A visual representation of the variables used in this model can be seen in Figure 3.2.

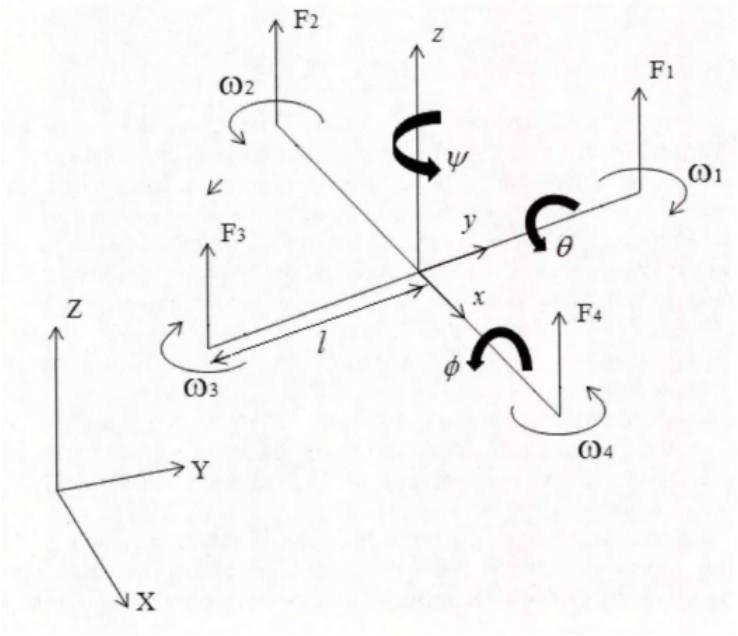

Figure 3.2: Mathematical Variables in a Quadcopter Model [15]

A reference frame (X, Y, Z) and a body frame (x, y, z) are used to describe the motion of the quadcopter. The angular speeds of the propellers are denoted by ω_{1-4}, and the upward thrust forces produced by each of the propellers are represented by F_{1-4}. The roll, pitch, and yaw angles are defined as ϕ, Θ and ψ, respectively. By using Euler Angles, a transformation matrix R can be obtained between the reference and body frame by rotating the model along the roll (ϕ), pitch (Θ), and yaw (ψ) axes. Equation 3.0 effectively describes the rotation of the rigid body (quadcopter) about the reference frame [15].

$$\Big[R\Big] = \begin{bmatrix} c(\Theta)c(\psi) & s(\phi)s(\Theta)c(\psi) - c(\phi)s(\psi) & c(\phi)s(\Theta)c(\psi) + s(\phi)s(\psi) \\ c(\Theta)s(\psi) & s(\phi)s(\Theta)s(\psi) - c(\phi)c(\psi) & c(\phi)s(\Theta)s(\psi) - s(\phi)c(\psi) \\ -s(\Theta) & s(\phi)c(\Theta) & c(\phi)c(\Theta) \end{bmatrix} \tag{3.0}$$

Where “c” represents *cos* and “s” represents *sin*.

The linear motion of the quadcopter in flight can be described by Equation 3.1. The rotation matrix R is used to map thrust vector T_B from the body frame to the inertial frame [18].

$$m\vec{x} = \begin{bmatrix} 0 \\ 0 \\ -mg \end{bmatrix} + RT_B + F_D \tag{3.1}$$

Where:

$\vec{x}$: is the position of the quadcopter

m : is the mass of the quadcopter

g : is the acceleration due to gravity

F_D : is the drag force

T_B : is the total thrust produced by the four propellers

Both equations 3.0 and 3.1, among others, can be used to describe the behaviour of a quadcopter in flight. By implementing these equations, the performance of a quadcopter can be simulated in software under varying conditions.

PID Response

PID control systems are designed to limit the disturbance of external variance. In the case of a quadcopter, PID controllers are used to obtain a desired positional or thrust state of the craft. To evaluate the performance of the PID controller, certain parameters are assigned to the response as seen in Figure 3.3 below [8].

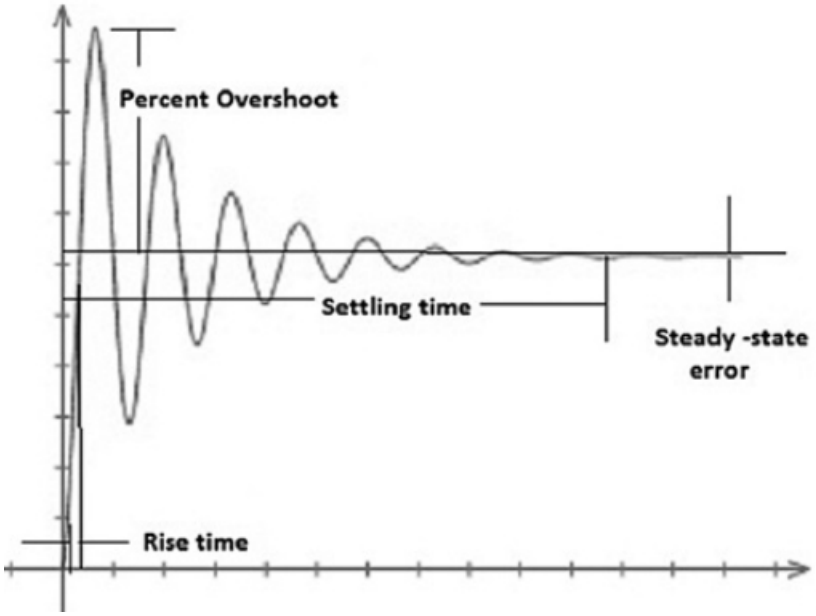

Figure 3.3: PID Response Graph [8]

Rise time is the time it takes for the response to rise from 10% to 90% of the final (steady state) value. **Settling time** is the time it takes for the response to settle to within a certain percentage of the steady state value, usually 5%. **Percent overshoot** is the maximum response value obtained, expressed as a percentage compared to the steady state value. **Steady state error** is the difference between the actual and ideal output [8].

Simulation Overview

Simulation was conducted using MATLAB Simulink. A software collection called "Quadcopter Dynamic Modeling and Simulation" was used to generate the required outputs based on the pure theoretical aspects of the quadcopter operation. A more direct, simplified linear model was used to simulate the behavior of the quadcopter as a function of time. [[]This system contains PID implementation, RC control inputs, and quadcopter state outputs [16]. A simplified overview of the system components of interest can be seen in Figure 3.4.

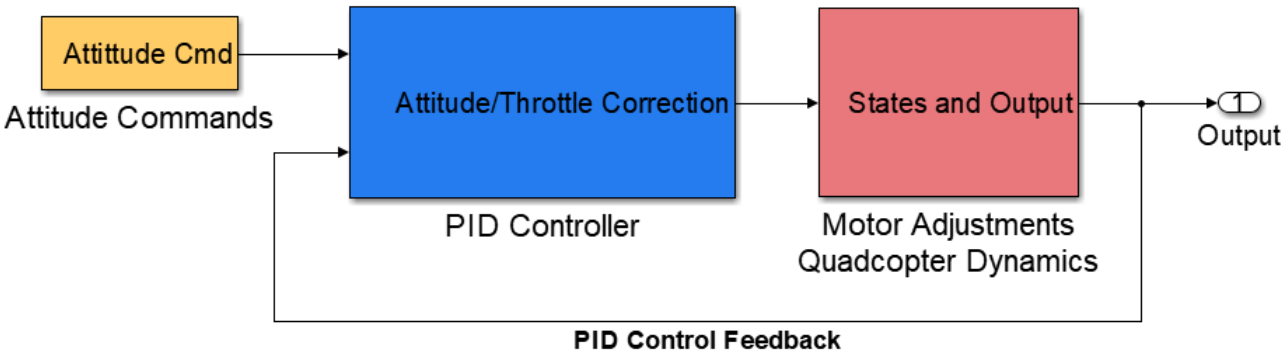

Figure 3.4: Quadcopter Simulator [16]

Each axis contains its own PID controller, and any corrections applied are translated into motor speeds. Based on a quadcopter model similar to the one used experimentally, different simulated state outputs were obtained to describe an ideal performance.

3.3 Altitude Hold

To maintain a set altitude above ground level, the control axis of primary concern is thrust. Essentially, the throttle command must be varied appropriately to maintain a steady altitude. This is achieved through the use of a PID controller which uses the error between the desired altitude and current altitude to adjust the throttle accordingly. A block diagram of the Simulink model used for simulation can be seen in Figure 3.5 below [16].

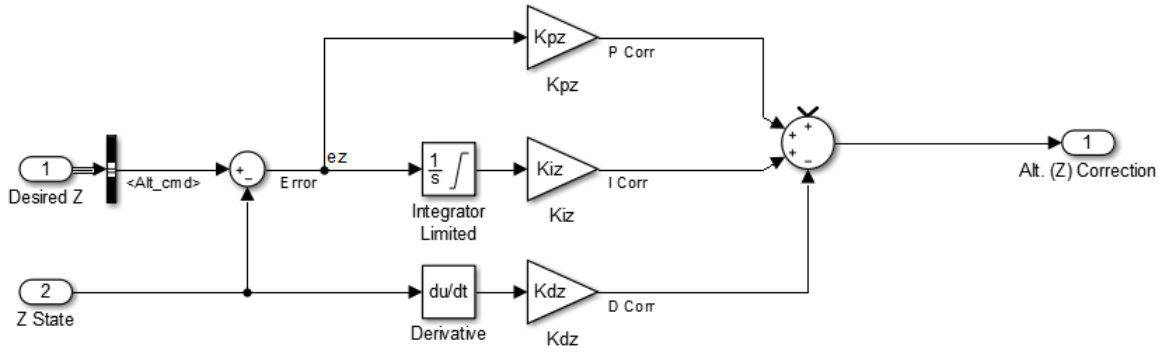

Figure 3.5: Simulation Altitude PID [16]

As described in section 2.1.2, the proportional, integral, and derivative correction blocks are present and have gains associated with each. The input to this control system is the error generated by the difference of the desired altitude ("Z") and the current altitude. The current altitude relies solely on the mathematical model which describes the inertial behaviour of the quadcopter as it flies. One way to interpret this value is to treat it as "ideal" sensor data, in that it describes the measured above ground level (AGL) based solely on the results of the simulated quadcopter vertical motion. The output of this system is a corrective adjustment that is sent to the motors, adjusting the overall thrust based on the feedback produced by the current altitude measurement [16].

To evaluate the PID controller, a steady hover state at a desired altitude was achieved. Then, an immediate discontinuity in the AGL measurement was introduced, allowing for the observation of a step response of the PID controller. For the simulation, this was achieved by generating a single pulse input for the altitude command, which effectively caused the simulated quadcopter to suddenly increase altitude, hover, and then suddenly decrease alti-

tude. This allows for the observation of the PID step response for both a rising and falling edge discontinuity.

To evaluate the PID controller implemented on the actual quadcopter, the PID gains were set to equivalent proportions. Also, the current altitude state used for the error calculation relied on the distance measured by the LEDDAR sensor. A step response of the implemented PID algorithm was observed by introducing a 30 cm high rectangular obstruction underneath the quadcopter during a stable hover state.

The true altitude of the quadcopter was obtained by recording a video of the flight and placing a measurement tape in the background for reference. Every 5 frames of the 30 frame per second video was processed and the height was recorded for each frame. This means that a height measurement independent of the quadcopter system was obtained approximately every 167 ms. A sample frame of the video used for data collection can be seen in Figure 3.6.

Figure 3.6: Ground Truth Data Collection

The true altitude of the quadcopter (ground truth data) was obtained and compared to the simulated altitude as seen in Figure 3.7 (a larger version of the plot is available in the Appendix).

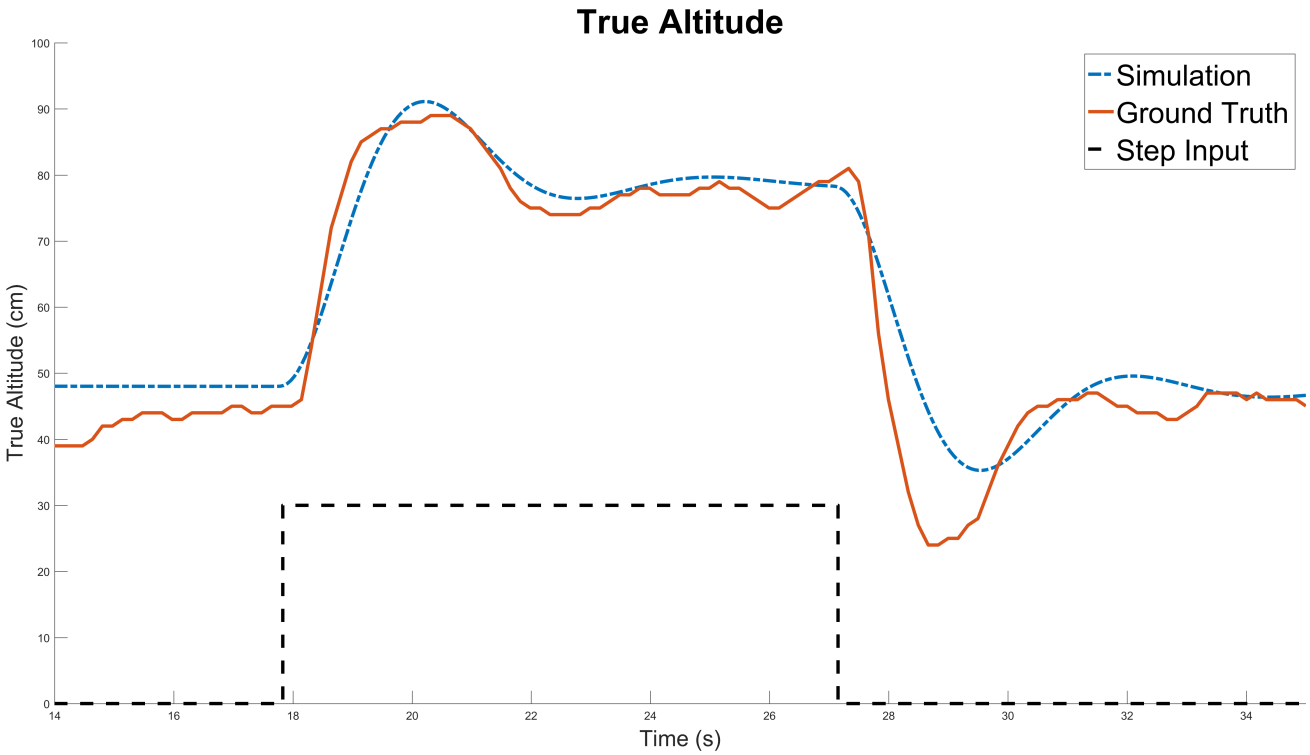

Figure 3.7: Altitude Step Response

The 30cm high rectangular obstruction suddenly placed underneath the hovering quadcopter is represented by the dashed line. This can be interpreted as the step input introduced to the control system, where the rising edge occurs around 17.8 seconds and the falling edge occurs around 27 seconds. The simulation results are represented by the dot-dash line and can be considered the ideal altitude response of the quadcopter. This is directly compared to the solid line, which represents the ground truth data. The ground truth data was acquired externally, meaning that this altitude data did not rely on the LEDDAR sensor measurements. It can be interpreted as the actual altitude of the quadcopter during flight. One notable observation is the steady state error of the ground truth altitude compared to the simulation. However, the scaling of the graph shows that this error only ranges between about 3 cm to 10 cm, which is insignificant for this application, especially considering the size of the quadcopter.

The response of the PID controllers are very similar, except for the different in steady state altitudes. Table 3.1 compares the step response metrics between the simulation and

ground truth data, as described in section 3.2. Much of the error can be accounted for by the slightly different flight models between the simulated and physical quadcopter, sensor data variability resulting in a non-ideal step response, and the introduction of air turbulence in the test area.

Table 3.1: PID Performance Metrics

	Simulation	**Experimental**
Rise Time (s)	0.92	0.60
Settling Time (s)	26	26.04
Percent Overshoot (%)	27.3	17.02
Steady State Error (%)	0	4.2

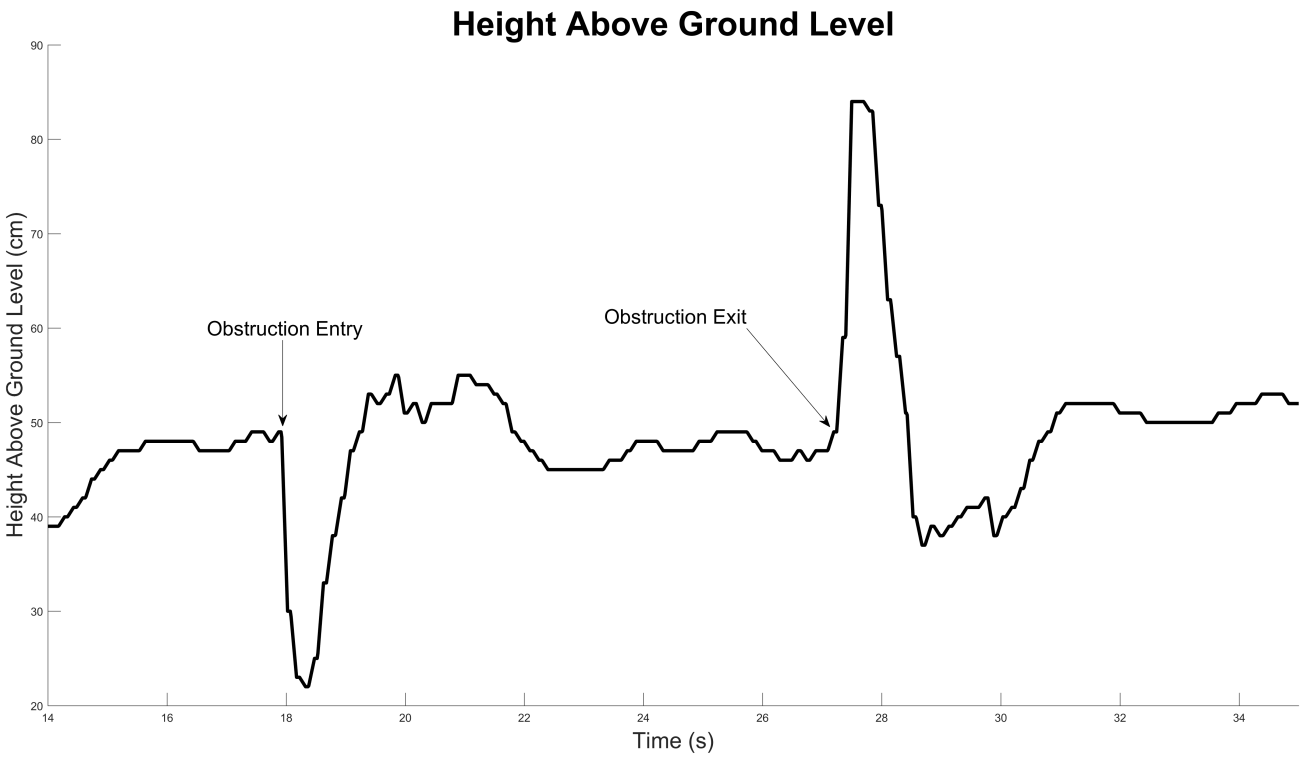

Figure 3.8: Height Above Ground Level Step Response

Another useful plot can be seen in Figure 3.8, which shows the step response of the height above ground level. Height above ground level is the distance between the quadcopter and the ground directly beneath it. In this scenario, it can be interpreted as the data acquired from the LEDDAR sensor. This means that it directly represents the altitude measurement from the perspective of the quadcopter, and this altitude data is used in the PID control algorithm. Ideally, this height measurement should stay the same during flight. As the step input is introduced ("Obstruction Entry"), the height above ground level measurement suddenly decreases by roughly 30 cm. This can also be observed on the falling edge of the step input ("Obstruction Exit"), where the height above ground level suddenly increases by about 30 cm due to the removal of the obstruction.

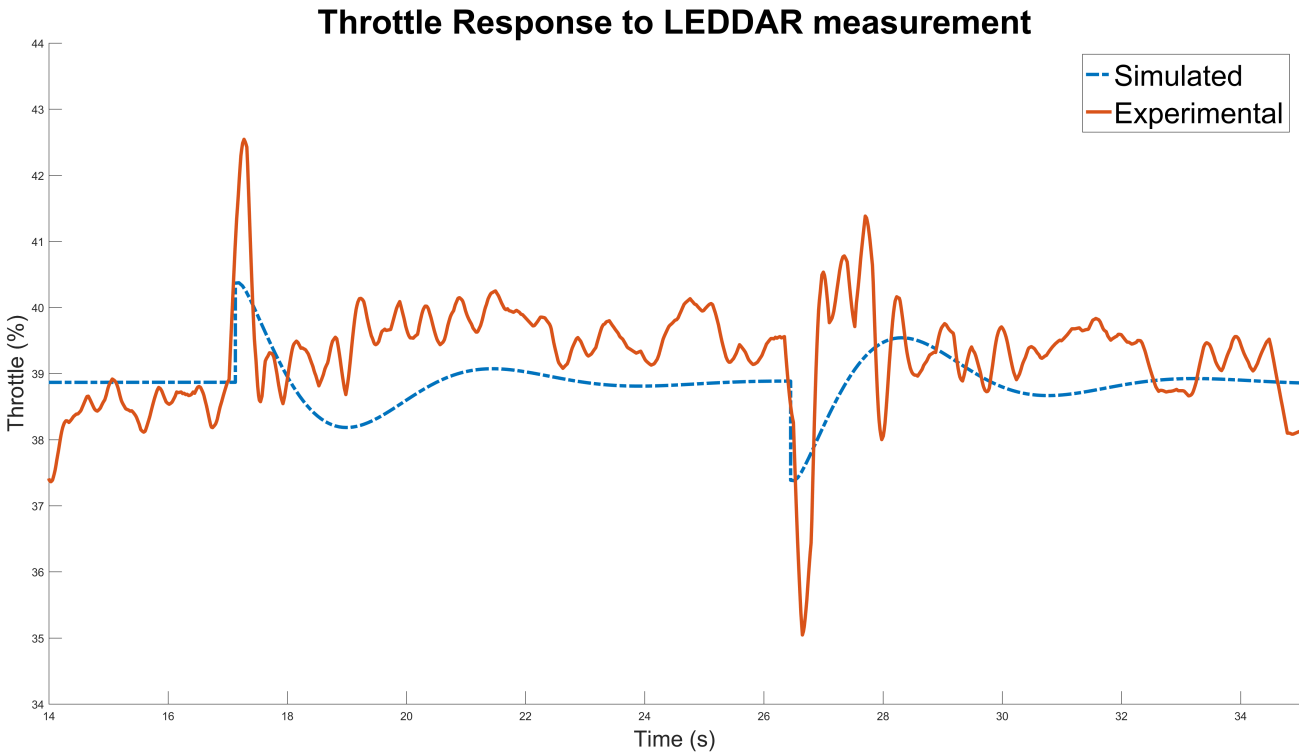

Figure 3.9: Throttle Step Response

Another way to observe the PID response is to view the throttle commands sent to the motors. This effectively represents the PID controller's step response to the sudden change in height above ground level. In Figure 3.9, the throttle commands generated in simulation and testing are compared. The dashed line represents the simulated throttle while the solid line represents experimental throttle. This comparison brings the differences between a simulation and reality into stark contrast. Though it is clear that the two spikes in throttle on the rising and falling edge of the pulse are present in both, the throttle commands at steady state are much more varied in the experimental data. Once again, this can be caused by numerous factors present in reality that are nonexistent in simulation.

3.4 Wall Avoidance

The roll control axis is used to maintain a set distance from a wall on the right side of the quadcopter. This means that the side to side movement of the quadcopter along the Y axis (see Figure 3.2) is used to control its distance relative to the wall. Just as in the altitude hold configuration, a PID control scheme is used for roll corrections during flight. The simulation mode can be seen in Figure 3.10 below [16].

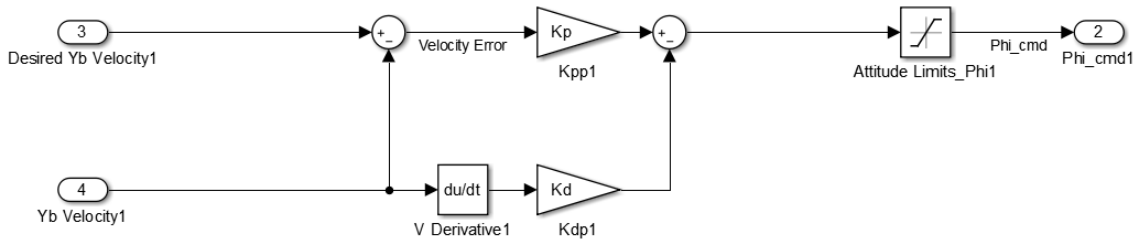

Figure 3.10: Simulation Roll Controller [16]

The PD controller in Figure 3.10 is used to generate the ϕ, or roll commands as if they were sent from the remote controller. The output of the controller "Phi_cmd1" is then sent to the full PID controller similar to the throttle control system in Figure 3.5. The simulated error signal, "Velocity Error," is representative of the velocity of the quadcopter, in that the position error of the quadcopter is mapped to a desired velocity towards or away from the wall. This desired velocity is then directly translated to a corresponding angle, or attitude, command "Phi_cmd1." If there is a sudden change in the target position Y, the desired velocity would be updated to reflect the angle of the quadcopter towards or away from the steady state [16]. It should be noted that there is no integral element in the simulated controller. The proportional and derivative control account for the velocity error and acceleration, respectively, and adequately respond to changes in velocity.

To evaluate the PD controller implemented on the quadcopter, the control gains were set to equivalent proportions. With the quadcopter initialized at a steady state distance Y_{ss} away from the wall, a step input with a rising and falling edge was simulated. A target distance Y_{target} was used to represent the step input by adding the obstruction offset to Y_{ss}. The size of the step used in the simulation represents the depth of a rectangular obstruction suddenly

placed in front of the LEDDAR sensor, which would cause the quadcopter to adjust its true position relative to the wall. For instance, if the quadcopter was maintaining a distance of 70 cm from the wall (Y_{ss}), a 30 cm obstruction placed between the sensor and the wall would cause the quadcopter to ideally reach a distance of 100 cm relative to the wall (Y_{target}). This same approach was used to generate the falling edge of the step input by changing the desired distance from Y_{target} to Y_{ss}. The results of the simulated response can be seen in Figure 3.11 (a larger version of the plot is available in the Appendix).

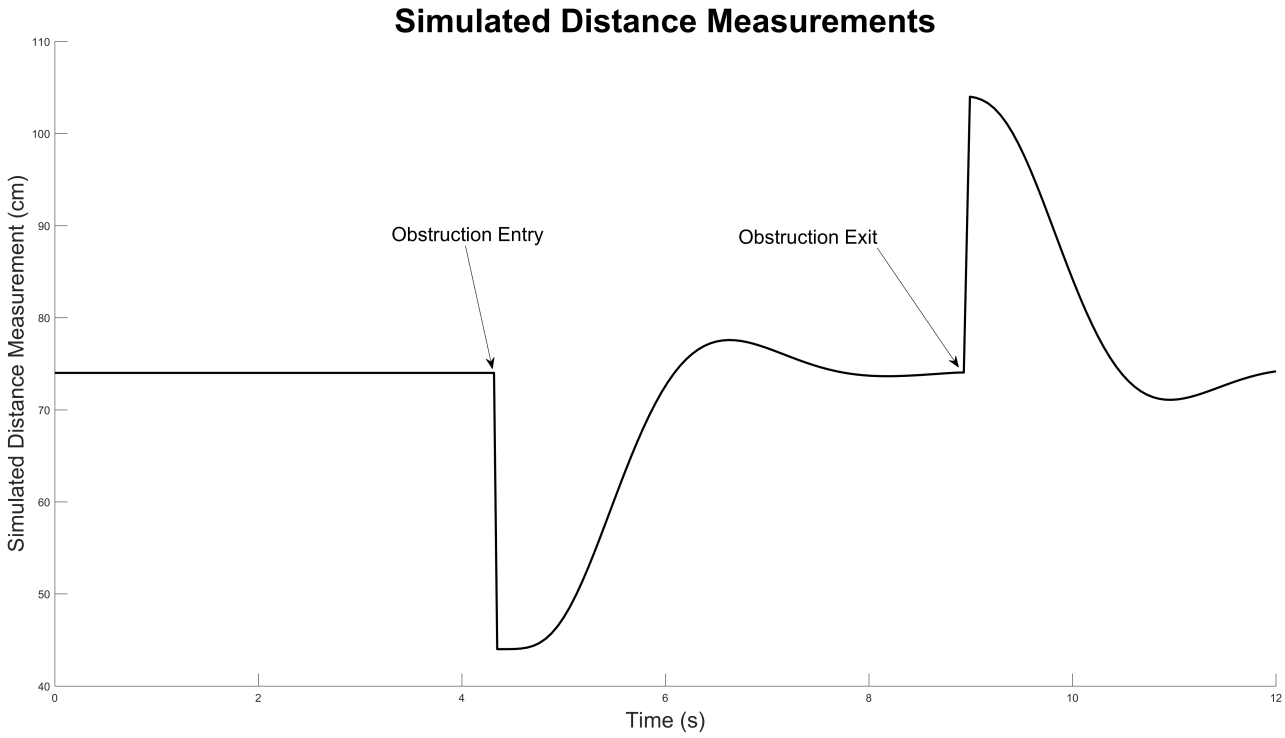

Figure 3.11: Simulated Roll Step Response

The above figure shows the simulated values of the distance to the wall as observed by the quadcopter. One way to interpret this is to view this plot as the ideal sensor measurements during the step response. The quadcopter initializes at a distance of 74 cm from the wall, and the points in time where the 30 cm obstruction is introduced and removed are labeled. Notice how the relative distance between the quadcopter and the measured distance always attempts to return to the initial distance of 74 cm.

A step response of the implemented control algorithm was observed by introducing and removing a 30 cm high rectangular obstruction in front of the wall during steady state distance holding. The results of the experimental test can be seen below in Figure **??** (a larger version of the plot is available in the Appendix).

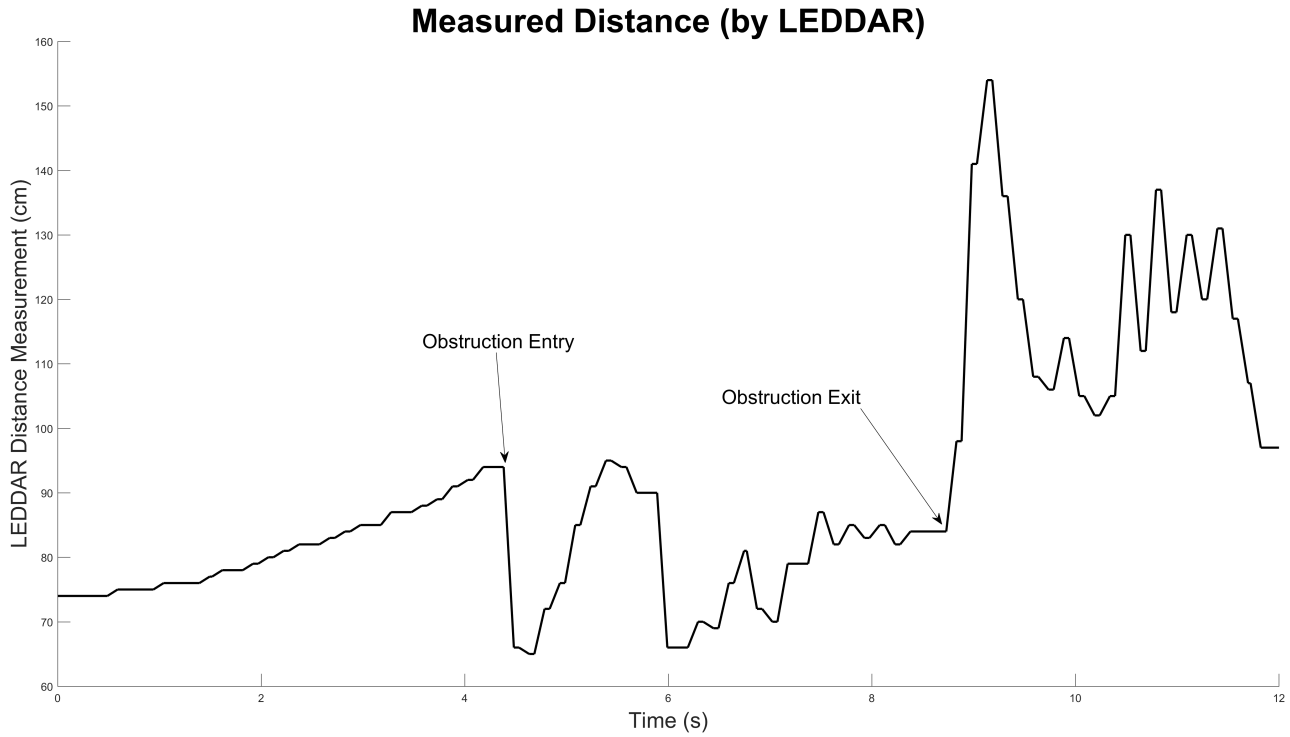

Figure 3.12: Experimental Roll Controller Performance

The above figure shows the distance measurements obtained by the side-mounted LEDDAR sensor. A system response can be observed at the labeled points where the obstruction entry and exit occur. A notable observation is the apparent inconsistency in the distance measurements, especially when compared to the altitude controller. During testing, a noticeable drift was observed, even without the distance holding algorithm active. One of the main causes of this is the inherent instability of the test quadcopter platform used, caused by a variety of factors including air turbulence, weight balancing, and IMU noise.

This drift can be seen during the first four seconds, in which the quadcopter moves from its initial distance of 74 cm to 93 cm. When the obstruction is introduced, the quadcopter quickly adjusts its distance away from the wall in an attempt to stabilize its relative distance

to the ideal value of 74 cm (Y_{ss}). However, the steady state values (6s - 9s) of the quadcopter are highly variable, ranging from 65 cm to 87 cm, with an average steady state value of 78 cm. On the falling edge of the step response, labeled as "Obstruction Exit," a similar behavior can be observed, in which the quadcopter struggles to return to Y_{ss}.

Table 3.2 below summarizes and compares the performance of the simulated and experimental controllers.

Table 3.2: Controller Performance Metrics

	Simulation	**Experimental**
Rise Time (s)	0.94	0.30
Settling Time (s)	5.56	8.17
Percent Overshoot (%)	3.43	21.7
Steady State Error (%)	0	7.8

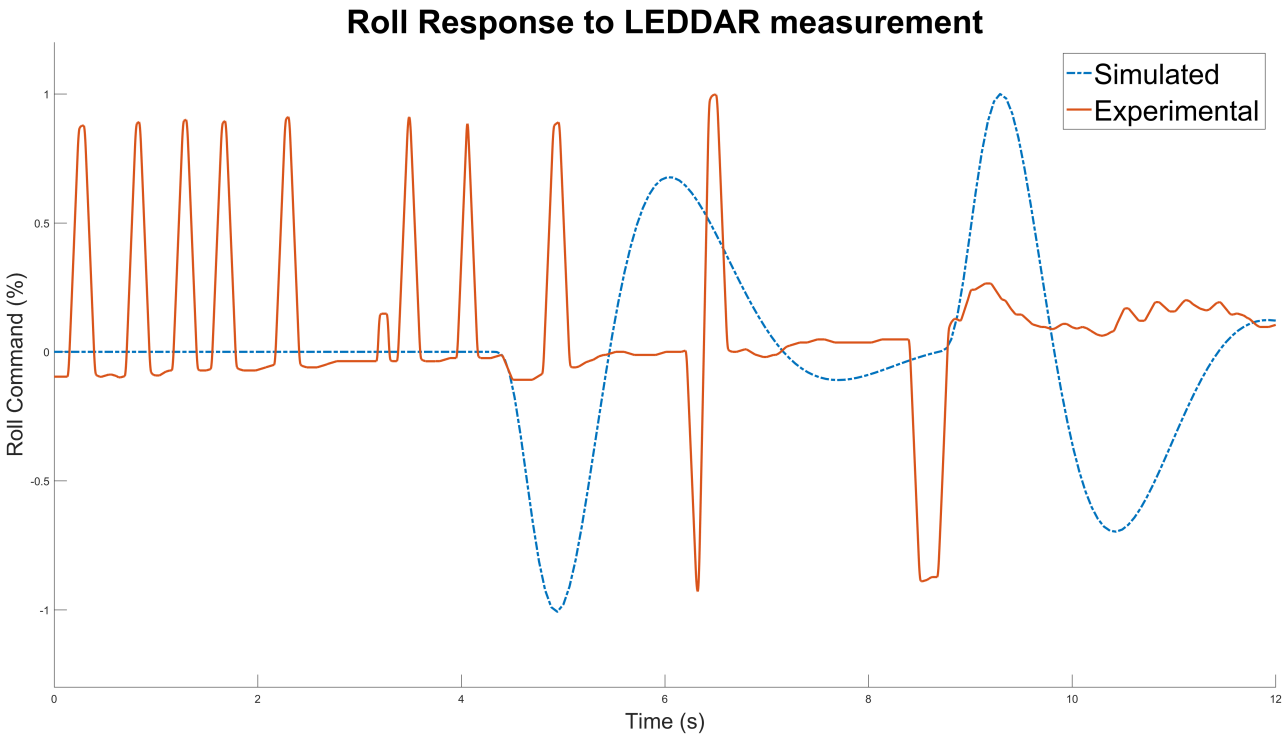

Figure 3.13: Roll Command Step Response

Another way to observe the step response is to view the roll commands sent to the motors. This effectively represents the controller's step response to the sudden change in wall distance due to the introduction and removal of the obstruction. In Figure 3.13, the roll commands generated in simulation and testing are compared. The dashed line represents the simulated roll while the solid line represents experimental roll. In the simulation, the command used to move the quadcopter away from the wall can be seen as a downward, then upward waveform. Similarly, to move back towards the wall an upward, then downward waveform is used. For both of these, the complimentary roll command is used to counteract the inertial motion of the quadcopter as it is moving towards or away from the wall. This effectively stops the quadcopter so that it will maintain its new position.

The experimental waveform follows this simulation to a minor extent, most notably around the 6 second mark. Though it is somewhat delayed, the same type of roll command can be seen to move the quadcopter away from the obstruction. To a lesser extent, this can also be seen in the roll command at 7 seconds when the obstruction is removed. The extra

roll commands from 0 to 4 seconds are likely a result of extraneous accelerometer data due to the IMU noise or platform instability, and are potentially one of the contributing factors to the initial drift in position observed in Figure 3.12.

Chapter 4

Conclusion

4.1 Summary

This research shows that it is possible to obtain spatial awareness and centering information for a quadcopter without GPS while operating in an underground mine. Compared to most currently explored solutions, the sensing approach used in this research provides a compelling compromise between weight, size, cost, power consumption, and system performance.

The capability of the quadcopter to alter its position based on the distance measurements provided by the light-based sensor was evaluated. Both the altitude above the current ground level and the distance from the current wall were used as inputs to the control systems. These controllers dynamically adjusted quadcopter commands to ensure the vertical and side distances were maintained during flight. The behavior of the quadcopter control system in response to a step input was simulated using a linear model, and then compared to the experimental results. In both the altitude and wall holding experimental tests, a steady state error of less than 10% was observed. In addition, the experimental response to the step input had a smaller overshoot than the simulation.

There were considerably more external disturbances in the test environment when compared to the simulation. Much of this can be accounted for by the nature of the physical quadcopter system, including flight dynamics, motors, propellers, distance measurement errors, and flight controller sensor data error (e.g., gyroscope, accelerometer). The performance

of the system was adequate when compared to the ideal performance, and it is reasonable to speculate that with more sensing capability and finer PID tuning full autonomy could be achieved to maintain the quadcopter position in the center of an entry.

4.1.1 Future Work

In a highly volatile environment like a collapsed mine, it would be beneficial for the quadcopter to have additional situational awareness beyond the scope of this research. A relatively minor addition to the configuration used in this research would be the addition of a second distance sensor on the other side of the quadcopter. This could be used to find the averaged horizontal distance between the two walls of the mine, and maintain the distance from both simultaneously. If weight, size, and power constraints could be accounted for, a laser scanning system similar to the research presented in [12] could be used to obtain a much higher resolution distance map of the surroundings. It could also be beneficial to investigate the use of other types of sensors, such as optical flow, IR, and sonar. Image processing techniques could even be used in conjunction with a camera, similar to the research in [14].

Furthermore, the wall position holding algorithm developed here could be modified to improve system performance by decreasing error and increasing stability response. It would also be extremely beneficial to reexamine the physical construction of the test quadcopter to improve stability and reduce sideways drift. A much more involved approach to navigation could utilize Simultaneous Localization and Mapping (SLAM) algorithms to obtain more autonomy. This is a highly popular research topic in the field of robotics, and is directly applicable to the navigation of a quadcopter in an underground coal mine.

Chapter 5

Appendix

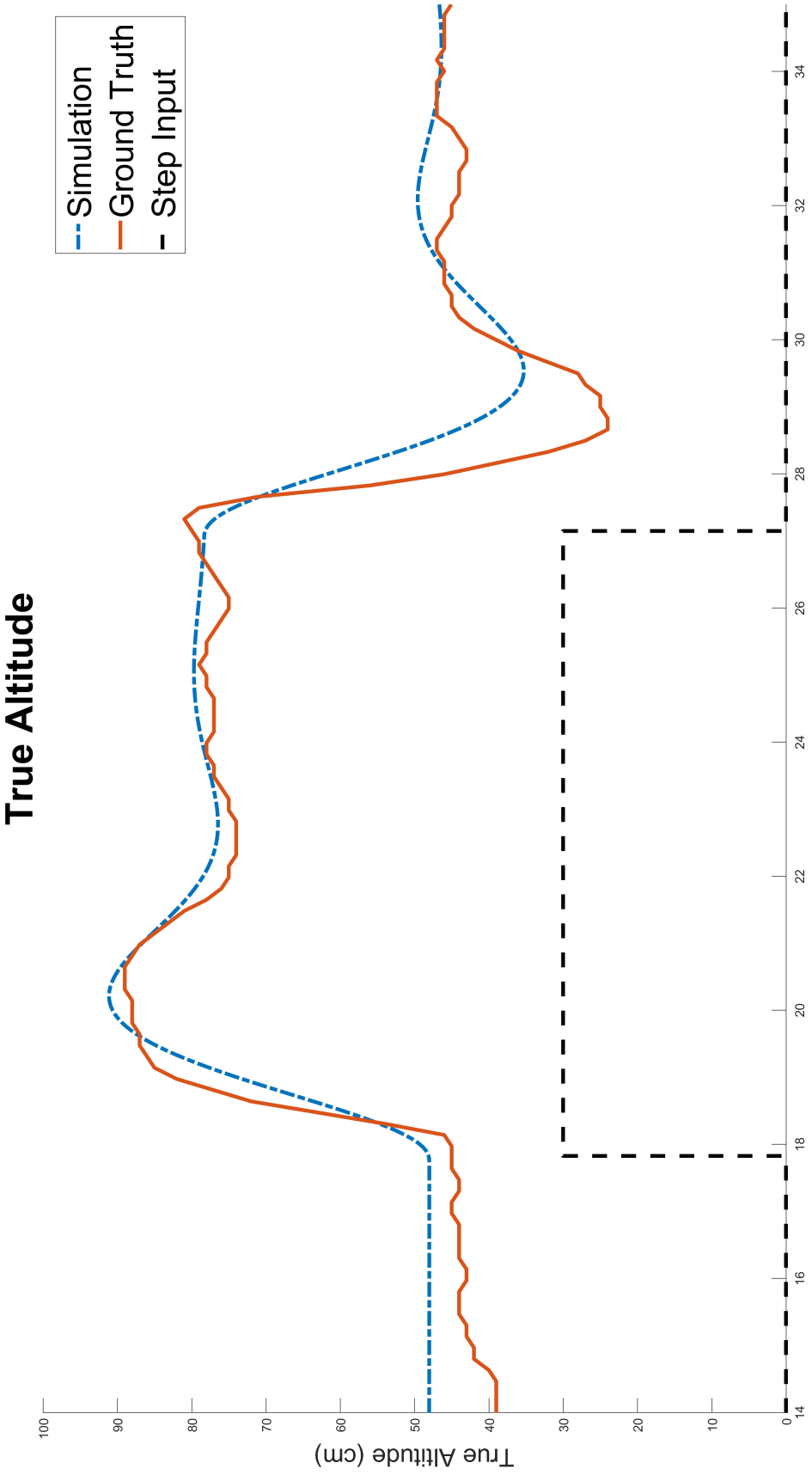

Figure 5.1: Altitude PID Step Response

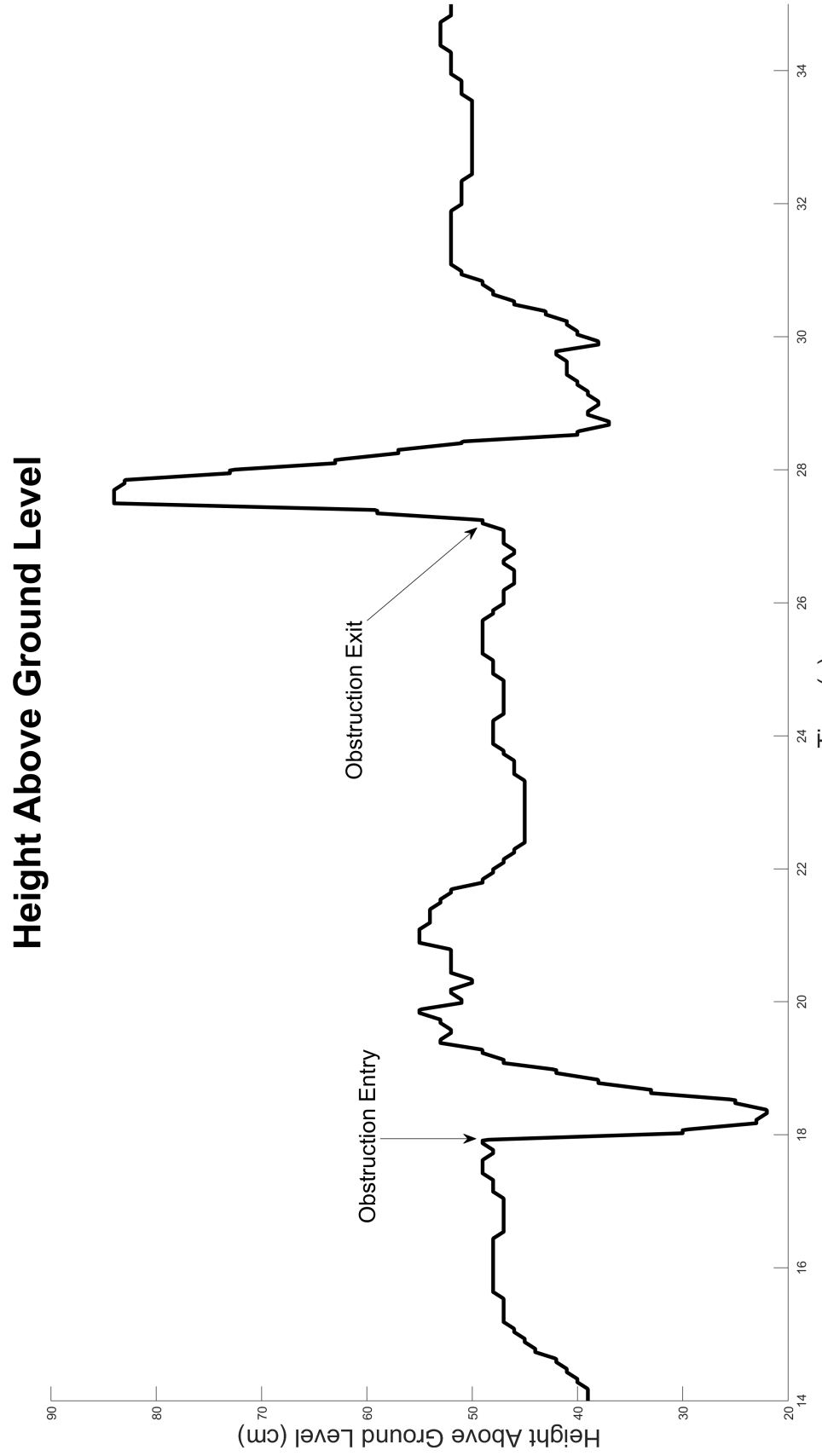

Figure 5.2: Height Above Ground Level Step Response

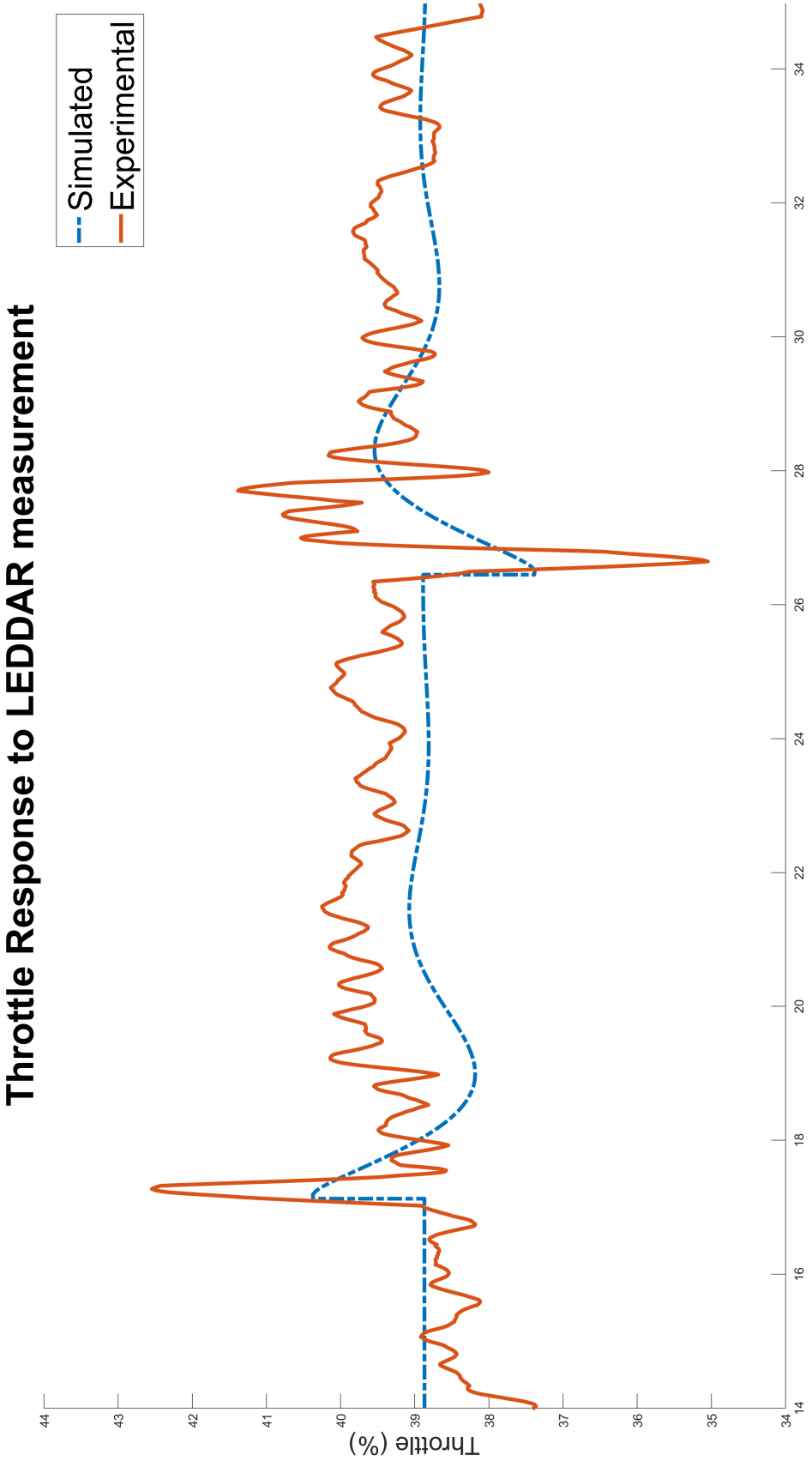

Figure 5.3: Throttle Step Response

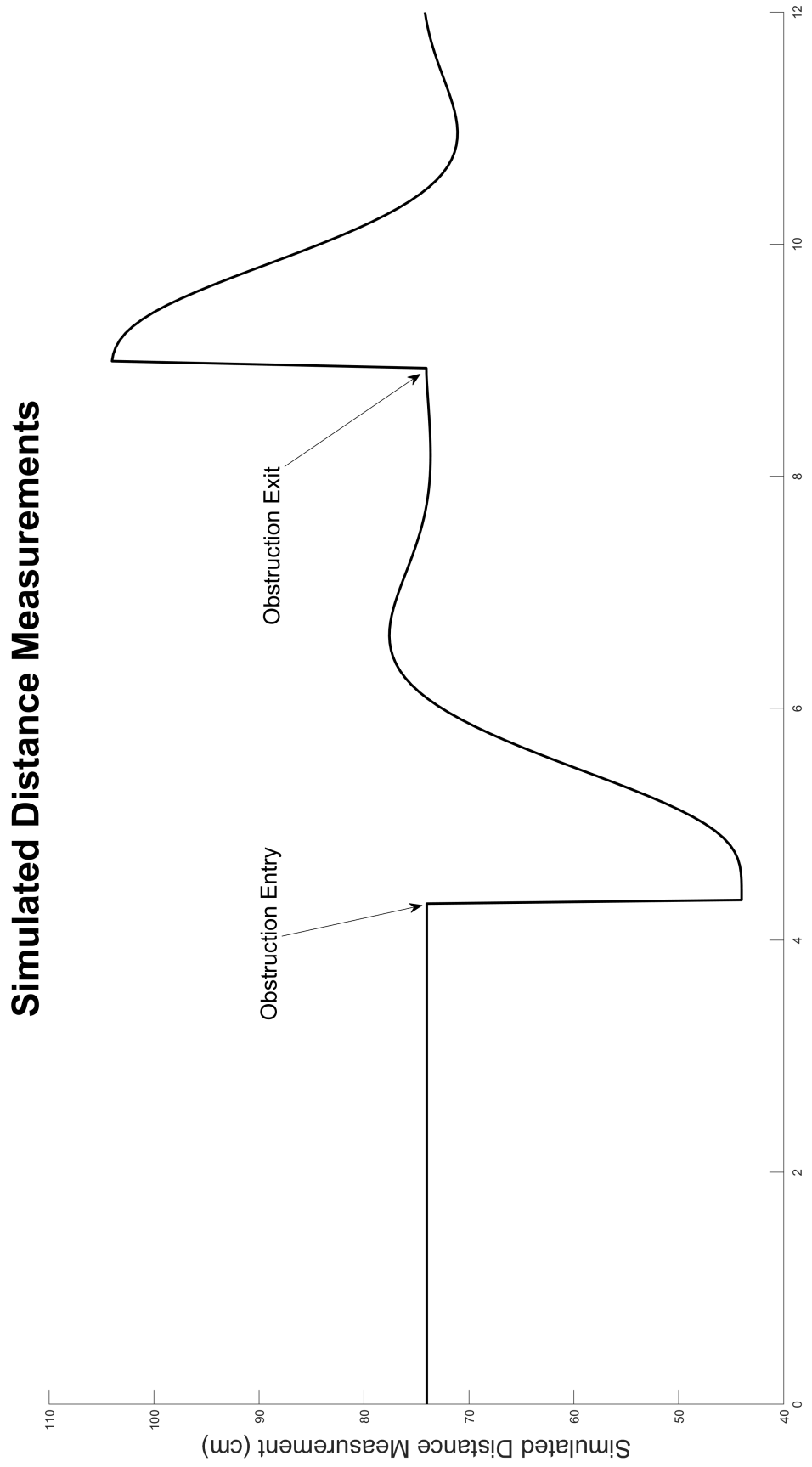

Figure 5.4: Simulated Roll Step Response

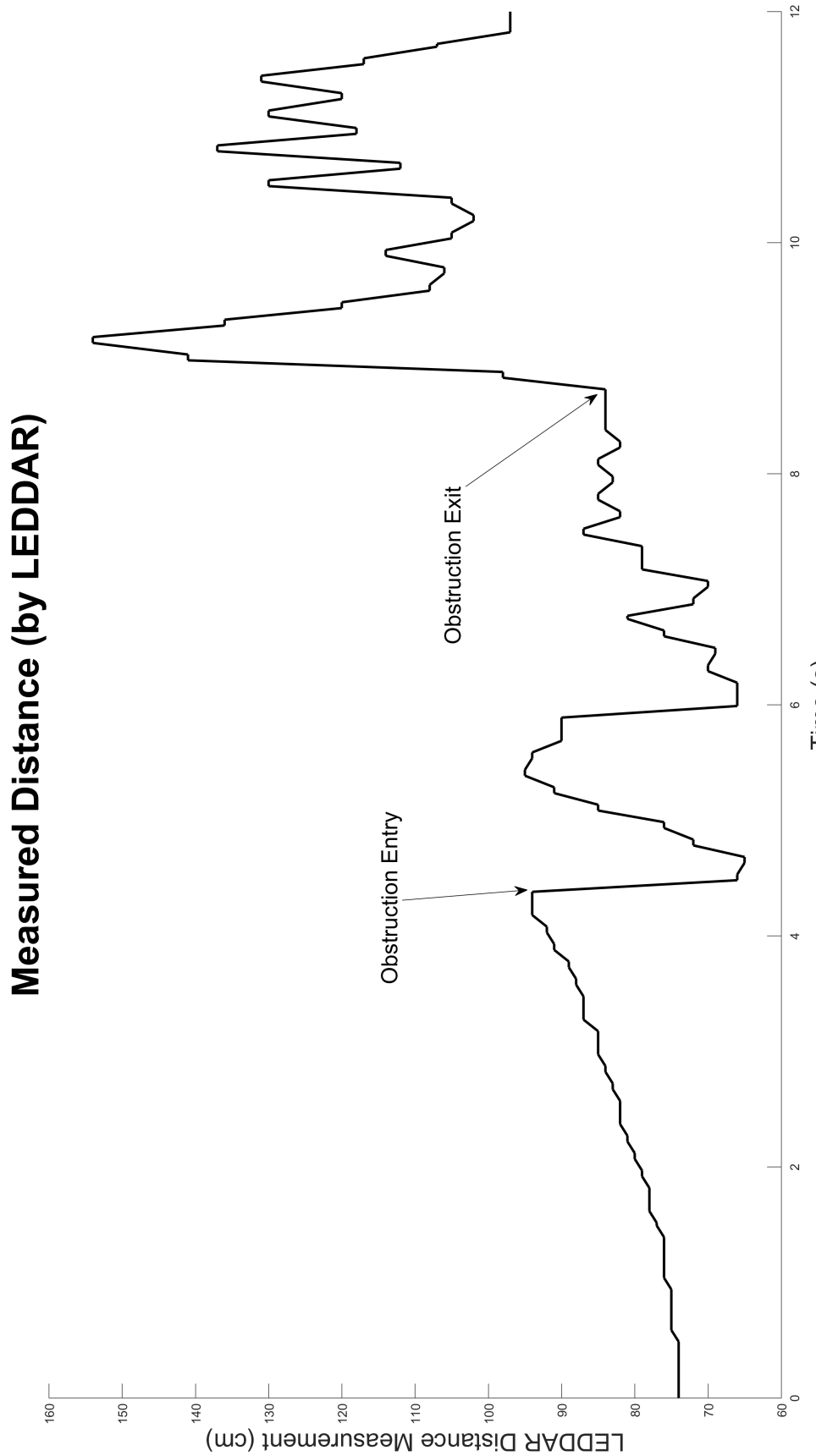

Figure 5.5: Experimental Roll Controller Performance

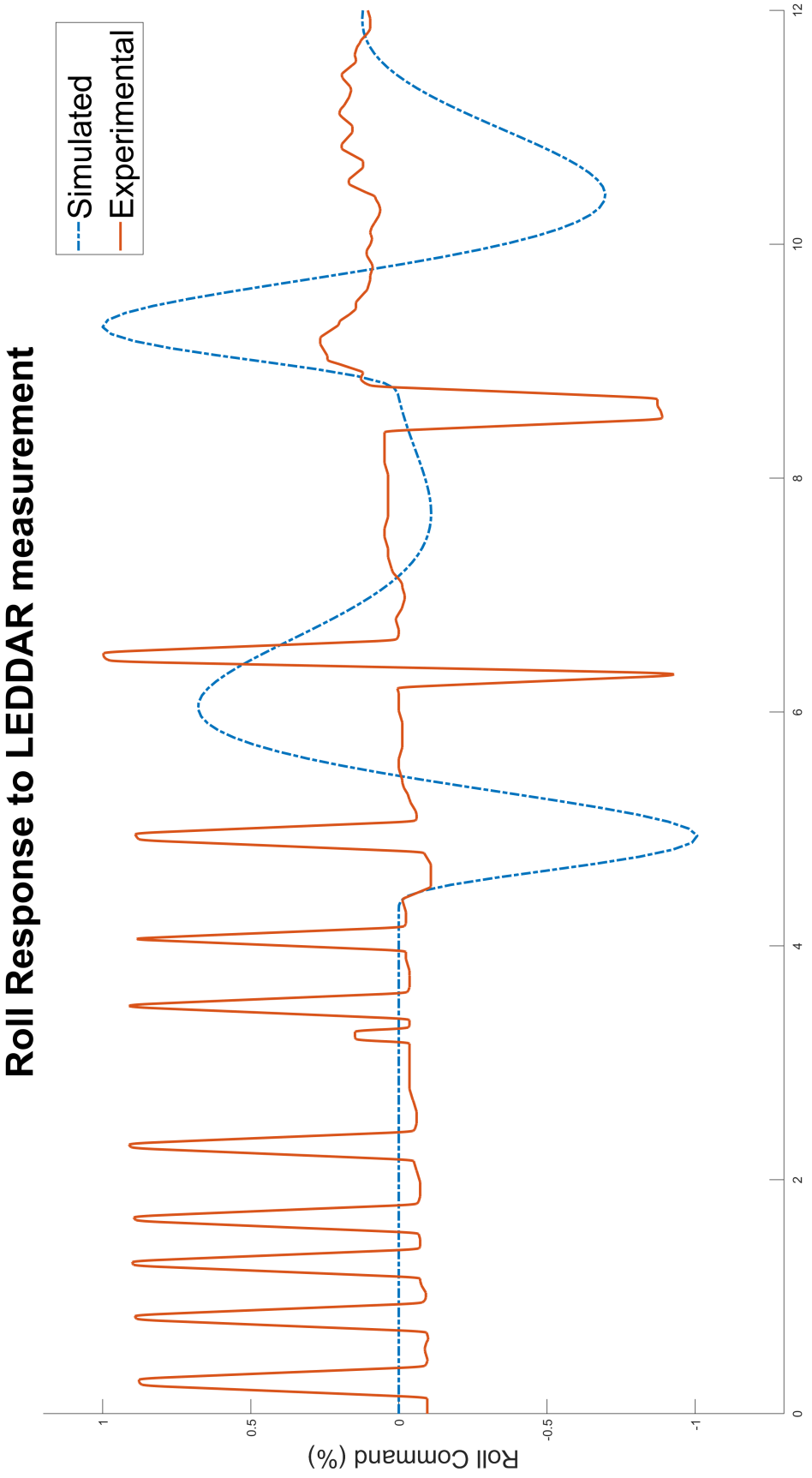

Figure 5.6: Roll Command Step Response

5.0.1 Down-hole Communications Overview

The objective of this project is to facilitate the above-ground operation of a quadcopter operating in a below-ground mine. Since the radio frequencies used to communicate joystick commands to the quadcopter will not penetrate deep enough into the ground, a different approach must be used to allow for this communication. In the context of mine rescue operations, a 6 to 8 inch diameter bore hole can be drilled as a means of access into the mine. This bore hole could be used as an entry point for a collapsible quadcopter, which could expand once deployed in the mine and explore the surrounding area. The focus of this project is to facilitate the communication link between the pilot operating the craft from the surface and the quadcopter flying in the underground mine. This includes the transmission of video data back up to the pilot on the surface.

The following off the shelf products were used to construct the demonstration system:

- Icron USB 2.0 Ranger 2211
- 9/125, Singlemode Fiber Cable, ST / ST, 1.0m
- Fiber Adapter, ST / SC (Rectangular Mounting), Bronze Alignment Sleeve
- TP-LINK MC210CS
- CAT 6 Ethernet Cable
- Mini HDMI – HDMI cable
- Camplex HDMI to Fiber Optic Extender
- Preterminated fiber optic cable (50 feet)

An overview of the entire system connections used for joystick control commands and video return can be seen in the following diagrams.

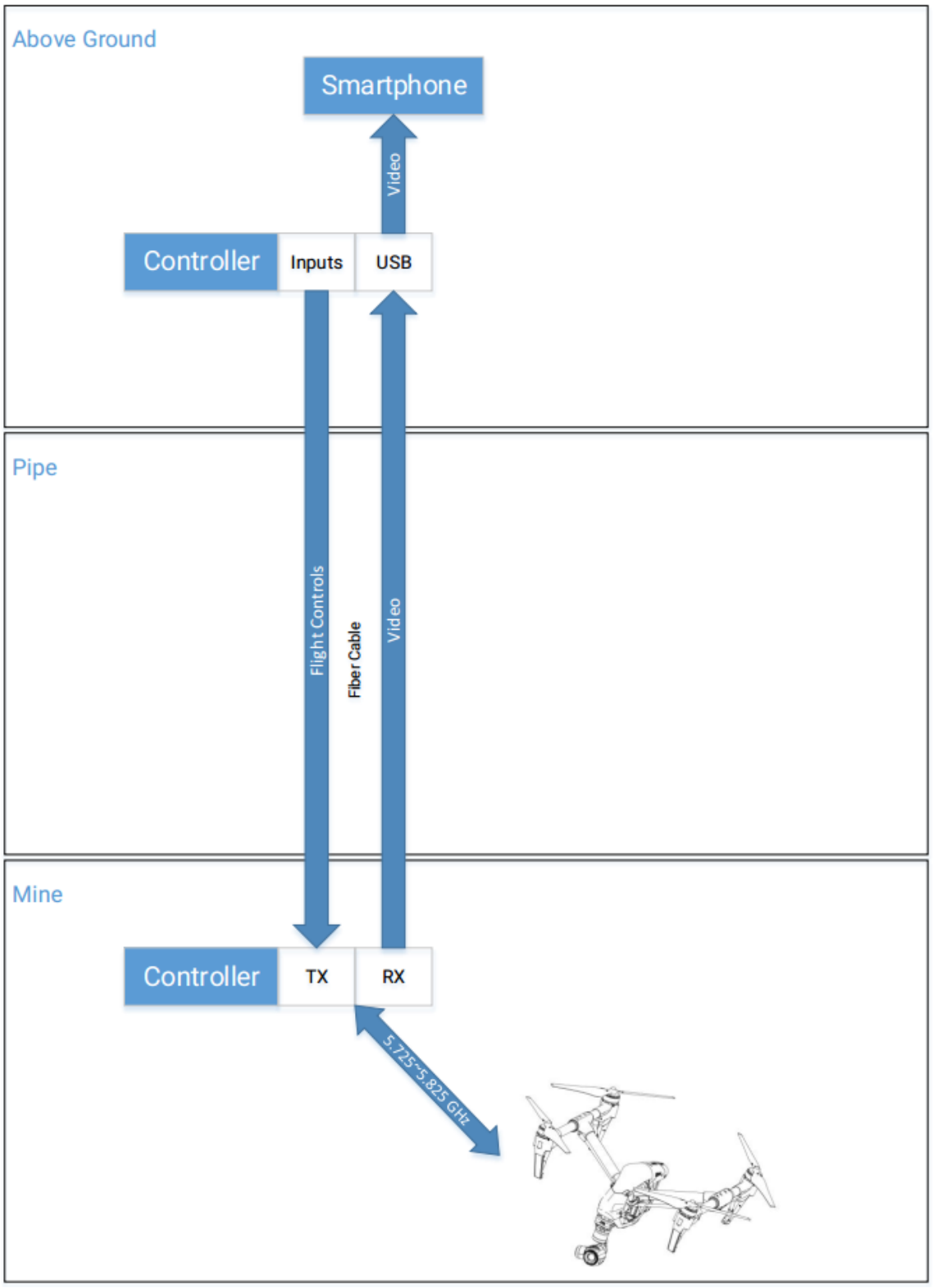

Figure 5.7: Overview of Fiber Optic Communication System

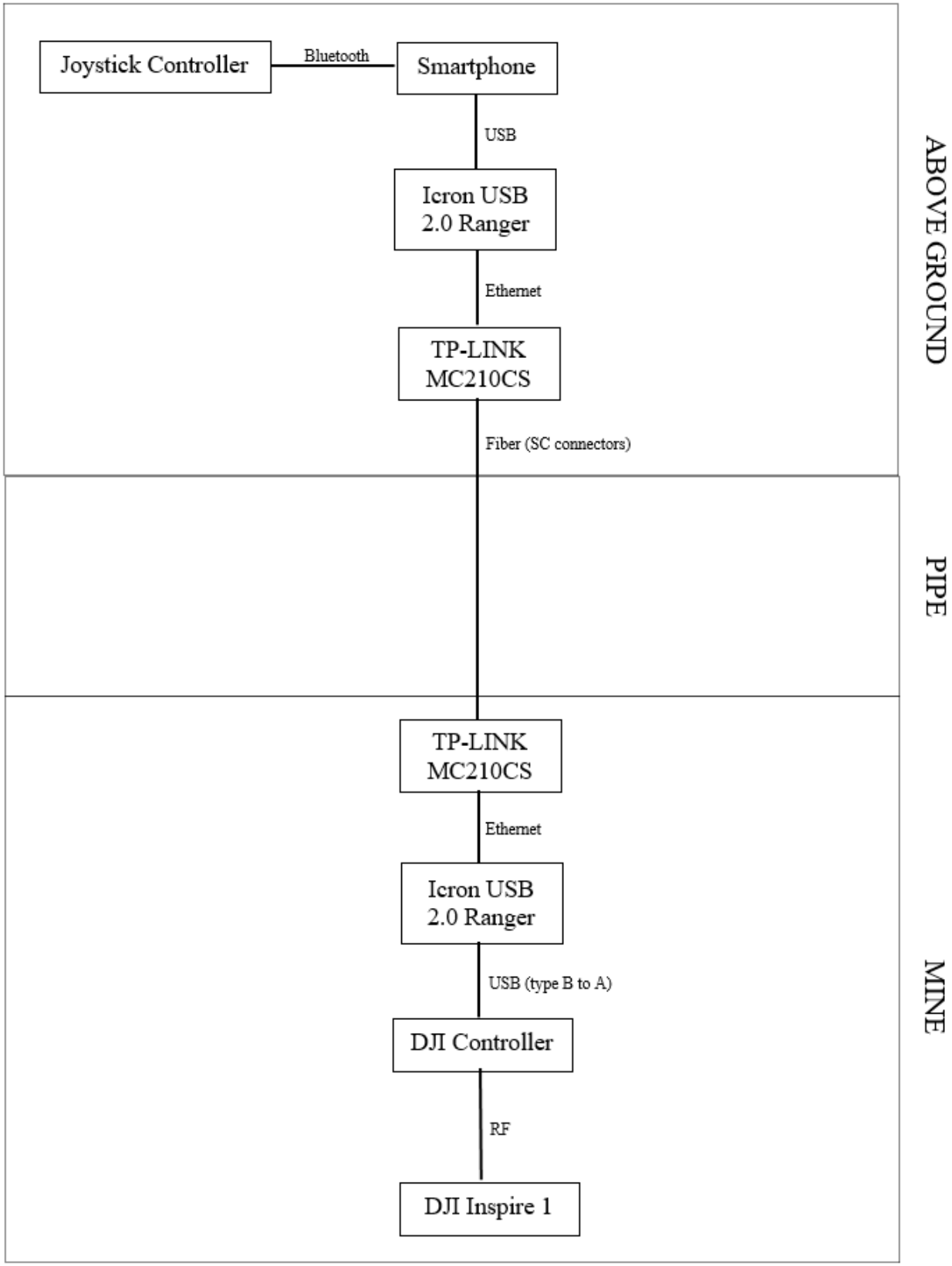

Figure 5.8: Connection Diagram of Control Communication over Fiber

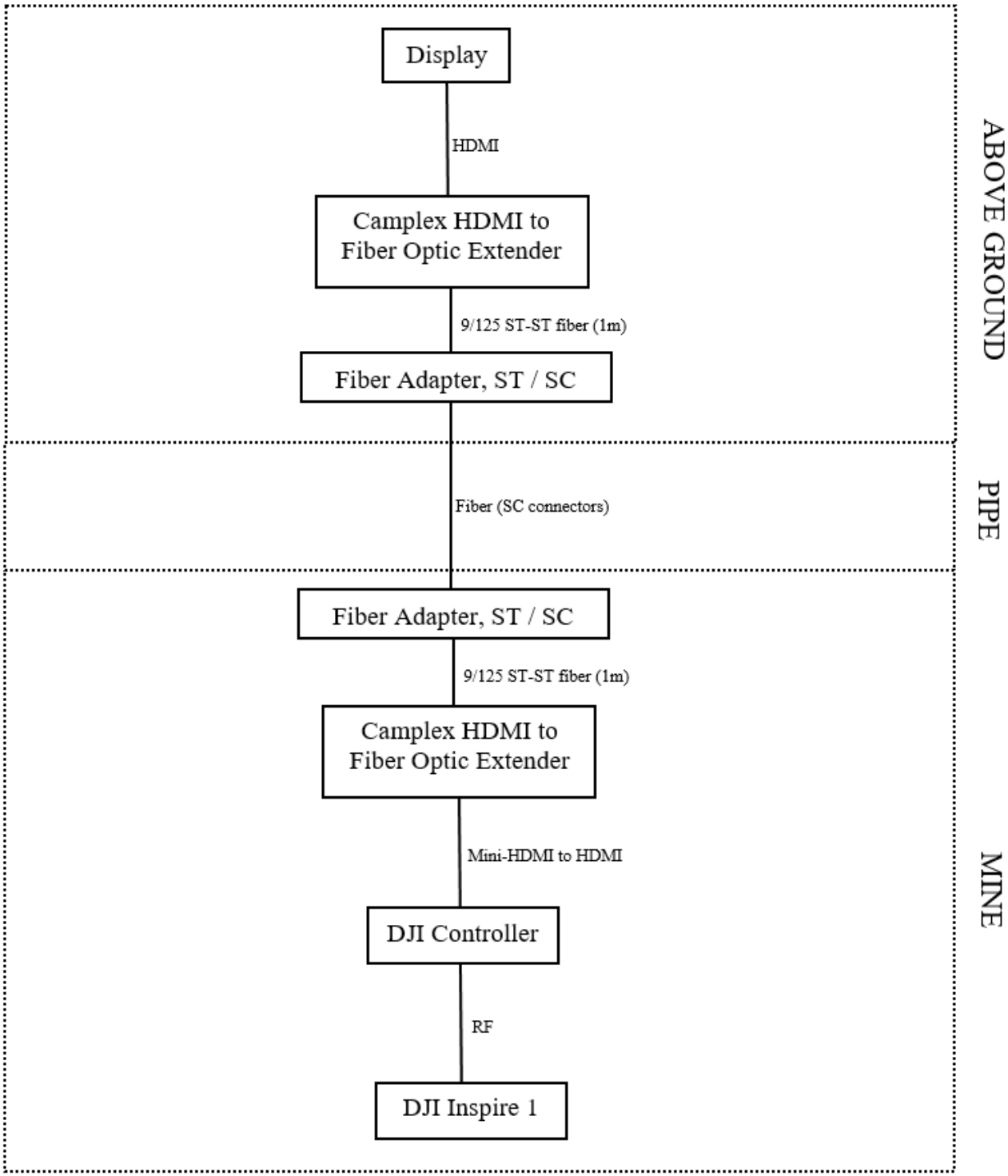

Figure 5.9: Connection Diagram of Video Communication over Fiber

References

[1] L. Inc., "Leddar™ One User Guide," Quebec, Canada.

[2] Parallax Inc., "PING)))™ Ultrasonic Distance Sensor (#28015)," pp. 1–12, 2009. [Online]. Available: https://www.parallax.com/sites/default/files/downloads/28015-PING-Documentation-v1.6.pdf

[3] Hokuyo, "Scanning Laser Range Finder Specifications," pp. 1–6, 2012, accessed on 07/16/2017. [Online]. Available: http://projects.asl.ethz.ch/datasets/lib/exe/fetch.php?media=hardware:tiltinglaser:utm-30lx-ln-specification.pdf

[4] Roy S Nutter, Jr., PhD, "2017 Proposal UAV Exporation (Concept Paper final), available by request from wvu through roy.nutter@mail.wvu.edu," 2017.

[5] Modbus Organization, "MODBUS Application Protocol Specification v1.1b3," Hopkinton, MA, 2012. [Online]. Available: Modbus-IDA

[6] D. Clifton, "Seriously Pro," 2015. [Online]. Available: http://seriouslypro.com/spracingf3

[7] B. T. M. Leong, S. M. Low, and M. P. L. Ooi, "Low-cost microcontroller-based hover control design of a quadcopter," *Procedia Engineering*, vol. 41, no. Iris, pp. 458–464, 2012. [Online]. Available: http://dx.doi.org/10.1016/j.proeng.2012.07.198

[8] Donald Norris, "Quadcopter Flight Dynamics," in *Build Your Own Quadcopter: Power Up Your Designs with the Parallax Elev-8*. McGraw-Hill Education, 2014, ch. 2.

[9] A. Visioli, "Basics of PID Control Closed loop control system," in *Practical PID Control*. Springer, 2006, ch. 1, pp. 1–18.

[10] L. N. Hung and L. S. Bon, "A quadcopter-based auto cameraman system," *VCACS 2016 - 2016 IEEE Virtual Conference on Application of Commercial Sensors, Proceedings*, 2017.

[11] G. Brooker, *Introduction to Sensors for Ranging and Imaging*. Raleigh, NC: SciTech Publishing Inc., 2011, ISBN: 9781891121746.

[12] L. Kaul, R. Zlot, and M. Bosse, "Continuous-Time Three-Dimensional Mapping for Micro Aerial Vehicles with a Passively Actuated Rotating Laser Scanner," *Journal of Field Robotics*, vol. 33, no. 1, pp. 103–132, 2016.

[13] W. Günthner, *Enhancing Cognitive Assistance Systems with Inertial Measurement Units*. Berlin, Germany: Springer, 2008, ISBN: 9783540769965.

[14] D. Scaramuzza, M. C. Achtelik, L. Doitsidis, F. Fraundorfer, E. Kosmatopoulos, A. Martinelli, M. W. Achtelik, M. Chli, S. Chatzichristofis, L. Kneip, D. Gurdan, L. Heng, G. H. Lee, S. Lynen, L. Meier, M. Pollefeys, A. Renzaglia, R. Siegwart, J. C. Stumpf, P. Tanskanen, C. Troiani, and S. Weiss, "Vision-Controlled Micro Flying Robots," *IEEE Robotics & Automation magazine*, no. September, pp. 26–40, 2014.

[15] F. Ahmed, P. Kumar, and P. P. Patil, "Modeling and simulation of a quadcopter UAV." vol. 23, no. 4 OP - Nonlinear Studies. 2016, Vol. 23 Issue 4, p553-561. 9p., p. 553, 2016. [Online]. Available: http://search.ebscohost.com/login.aspx?direct=true&site=eds-live&db=a9h&AN=119836746

[16] D. Hartman, K. Landis, M. Mehrer, S. Moreno, and J. Kim, "Quadcopter dynamic modeling and simulation (quad-sim)," https://github.com/dch33/Quad-Sim, 2014.

[17] B. Gross, "MaxSonar Operation on a Multi-Copter." [Online]. Available: http://www.maxbotix.com/articles/067.htm

[18] A. Gibiansky, "Quadcopter Dynamics , Simulation , and Control Introduction Quadcopter Dynamics," pp. 1–18, 2012. [Online]. Available: http://andrew.gibiansky.com/blog/physics/quadcopter-dynamics/

[19] CleanFlight, "CleanFlight manual," pp. 1–68, 2016. [Online]. Available: https://github.com/cleanflight/cleanflight/tree/master/docs

[20] R. Zlot, M. Bosse, K. Greenop, Z. Jarzab, E. Juckes, and J. Roberts, "Efficiently capturing large, complex cultural heritage sites with a handheld mobile 3D laser mapping system," *Journal of Cultural Heritage*, vol. 15, no. 6, pp. 670–678, 2014. [Online]. Available: http://dx.doi.org/10.1016/j.culher.2013.11.009

[21] J. Itschner, "Code used for test environment," https://github.com/Trumar/cleanflight-1, 2017.

Spatial Centering of a Quadcopter in an Underground Coal Mine

Jonathan Itschner

Thesis submitted to the
Benjamin M. Statler College of Engineering and Mineral Resources
at West Virginia University
in partial fulfillment of the requirements for the degree of

Master of Science
in
Electrical Engineering

Lane Department of Computer Science and Electrical Engineering

APPROVAL OF THE EXAMINING COMMITTEE

Powsiri Klinkhachorn, Ph.D.

Vinod K. Kulathumani, Ph.D.

Roy S. Nutter, Ph.D., Chair

Date